The *kpc-1* 3'UTR facilitates dendritic transport and translation of mRNAs for dendrite arborization of a mechanosensory neuron important for male courtship

Mushaine Shih[1], Yan Zou[1,2], Tarsis Ferreira[3], Nobuko Suzuki[1], Eunseo Kim[1], Chiou-Fen Chuang[1], Chieh Chang[1,4]

[1] Department of Biological Sciences, University of Illinois at Chicago, Chicago, Illinois 60607, USA;

[2] School of Life Science and Technology, ShanghaiTech University, Shanghai 201210, China;

[3] Division of Developmental Biology, Cincinnati Children's Hospital Research Foundation, Cincinnati, Ohio 45229, USA;

[4] Correspondence should be addressed to: chieh.chang1@gmail.com

Summary

A recently reported Schizophrenia-associated genetic variant in the 3'UTR of the human furin gene, a homolog of *C. elegans kpc-1*, highlights an important role of the furin 3'UTR in neuronal development(*1*). We isolate three *kpc-1* mutants that display abnormal dendrite arborization in PVD neurons and defective male mating behaviors. We show that the *kpc-1* 3'UTR participates in dendrite branching and self-avoidance. The *kpc-1* 3'UTR facilitates mRNA localization to branching points and contact points between sibling dendrites and promotes local protein synthesis. We identify a secondary structural motif in the *kpc-1* 3'UTR required for dendrite self-avoidance. Animals with *dma-1* receptor over-expression exhibit similar dendrite branching and self-avoidance defects that are suppressed with *kpc-1* over-expression. Our results support a model in which KPC-1 proteins are synthesized at branching points and contact points to locally down-regulate DMA-1 receptors to promote dendrite branching and self-avoidance of a mechanosensory neuron important for male courtship.

Introduction

PVD nociceptive neurons innervate *C. elegans* skin with elaborate dendrite arbors that respond to harsh mechanical stimuli(*2*). Dendrite arborization allows uniform sensory coverage of PVD neurons across the entire surface of the animal outside the head region. However, the mechanism underlying this process is still largely unknown.

Dendrite arborization in PVD neurons is restricted within a defined time frame by two intrinsic timing mechanisms(*3*) and is constrained spatially by two organizing principles: Escape (branch out) from the intermediate target (the trap zone) upon arrival at it and self-avoidance(*4–6*). Self-avoidance is a process in which self-recognition among neurites of a single neuron is followed by their repulsion from each other. This selective repulsion between dendrites of the same cell was originally observed in leech neurons and proposed to promote a uniform receptive field(*7*, *8*). Recent studies using *Drosophila* as a model showed that homophilic binding of Dscam1 proteins on sister branches of the same cell (MB or da neurons) promotes repulsive interactions between them, to ensure that they diverge and grow along separate pathways(*9–13*). Since the Dscam1 mutation does not completely disrupt dendrite self-avoidance in *Drosophila* and there is no Dscam1 homolog in *C. elegans*, studying PVD dendrite self-avoidance in *C. elegans* provides a unique opportunity to identify novel mechanisms of dendrite self-avoidance. Indeed, several known developmental pathways, including UNC-6 (netrin), MIG-14 (Wntless), and FMI-1 (Flamingo) signaling, have been implicated in PVD dendrite self-avoidance in *C. elegans*(*6*, *14*, *15*).

It was previously reported that guidance cues SAX-7 (L1CAM) and MNR-1 (Menorin) generated in the hypodermis (skin) established dendrite growth pathways and

39 instructed dendrite arborization for PVD neurons in *C. elegans*(*16*, *17*). PVD neurons first
40 grow two longitudinally extending 1° dendrites along the anterior-posterior (A/P) axis.
41 Orthogonal arrays of 2°, 3°, and 4° dendritic branches emerge sequentially in a manner that
42 alternates between the dorsal-ventral (D/V) and the A/P axes to produce an elaborate
43 network of sensory processes(*5*, *18*) (Fig. 1b). Skin cues, SAX-7 and MNR-1, and a
44 muscle-derived cue, LECT-2, are required for dendrite pattern formation through direct
45 interactions with the dendrite receptor DMA-1 to form a multi-protein receptor-ligand
46 complex(*16*, *17*, *19–21*).

47 We isolate mutants through genetic screens that display profoundly affected
48 dendrite branching and self-avoidance in PVD neurons. We identify mutations in the *kpc-*
49 *1* gene as being responsible for defective dendrite branching and self-avoidance phenotypes
50 through whole genome sequencing. *kpc-1* mutants display a significantly lower tertiary
51 branch avoidance index and a decreased sensory coverage in the skin compared to wild-
52 type animals. Although *kpc-1* has been implicated in dendrite self-avoidance and
53 arborization, the mechanism by which *kpc-1* regulates these processes is unknown(*4*, *22*,
54 *23*). KPC-1 encodes a proprotein convertase subtilisin/kexin (PCSK). Here, we show that
55 *kpc-1* functions in PVD neurons to regulate dendrite branching and self-avoidance via the
56 *kpc-1* 3'UTR. The *kpc-1* 3'UTR is required for *kpc-1* mRNA localization to distal and
57 higher-order dendrites and promotes its local translation. Although over-expression of *kpc-*
58 *1* causes greater self-avoidance, it does not limit initial dendrite outgrowth, which supports
59 a direct role for *kpc-1* in self-avoidance. *dma-1* over-expression also displays similar
60 secondary dendrite branching and tertiary dendrite self-avoidance defects that are
61 suppressed with *kpc-1* over-expression. Thus, DMA-1 is a potential KPC-1 target that

62 becomes down-regulated with increased KPC-1 activity. Our results suggest a model in
63 which KPC-1 proteins are synthesized at branching points and contact points between
64 sibling dendrites, leading to local down-regulation of DMA-1 receptors and the consequent
65 dendrite branching and self-avoidance.

66 **Results**

67 **Isolation of mutants that display profound self-avoidance defects in dendrites of PVD**
68 **neurons**

69 *C. elegans* PVD neurons extend a large and highly branched dendrite arbor directly
70 beneath the hypodermal surface that envelops the worms to mediate an avoidance response
71 to harsh mechanical force as well as to other noxious stimuli including temperature(*2*). The
72 elaborate dendrite branching patterns that PVD neurons display are constrained by two
73 organizing principles: dendrite branching(*4*) and dendrite self-avoidance. Self-avoidance
74 is an important neuronal process in which dendritic branches arising from a single soma
75 (also called isoneuronal) turn away from one another to minimize crossing and overlap and
76 to promote a uniform receptive field(*24*).

77 The self-avoidance in *C. elegans* is likely to provide new mechanistic insight into
78 the process as the well-known self-avoidance molecule Dscam(*9–13*)is absent from the *C.*
79 *elegans* genome. In order to uncover new mechanisms responsible for self-avoidance in *C.*
80 *elegans*, we screened approximately 9,500 genomes for mutants that displayed self-
81 avoidance defects in secondary and tertiary dendrites. These screens uncovered three
82 strong mutants (*xr47*, *xr58*, and *xr60*) that show profound self-avoidance defects in all
83 animals examined (n>200 each). *xr47* and *xr60* mutants showed an additional secondary
84 dendrite branching phenotype (a defect in the dendrite branching), which resulted in
85 significant reduced number of secondary branches in *xr47* and *xr60* mutants compared to
86 wild-type animals (Table 1). Despite displaying extensive defects in self-avoidance among
87 secondary and tertiary sibling dendrites, *xr58* mutants showed little secondary dendrite
88 branching defect (Fig. 1 a, c; Table 1). In wild-type animals, secondary dendrites that

89 initially contacted neighboring secondary branches retracted in order to form a regularly
90 spaced array of parallel branches (Fig. 1 a, b). In *xr58* mutants, many secondary dendrites
91 remained in contact with each other (Fig. 1c). In wild-type animals, tertiary dendrites
92 initially extended but later retracted once their termini come into contact with sibling
93 tertiary branches (Supplementary Fig. 1). In *xr58* mutants, many tertiary dendrites
94 remained in contact with their siblings long after arborization ended (Fig. 1c;
95 Supplementary Fig. 1), resulting in a significantly lower tertiary branch avoidance index
96 (TBAI) compared to the wild-type animals (Fig. 1d; TBAI: 0.38 in *xr58* mutants versus
97 0.93 in wild-type, $p<0.0001$). In wild-type animals, PVD dendrite arbors were fully
98 extended beneath the hypodermis and covered the areas from the posterior animal body to
99 right before the head region (Fig. 1f, Supplementary Fig. 2a, 2c, and 2d). In *xr58* mutants,
100 PVD dendrite arbors developed partially overlapping menorahs, causing decreased sensory
101 coverage of skin (Fig. 1f, Supplementary Fig. 2b, 2c, and 2d). We quantified sensory
102 coverage of skin by PVD dendrite arbors using two measurements, receptive field index
103 and length ratio of receptive field (Supplementary Fig. 2c, d). Both measurements showed
104 significantly reduced values in *kpc-1(xr58)* mutants compared to the wild-type animals
105 (Supplementary Fig. 2).
106

107 **Identification of responsible mutations in the *kpc-1* gene**

108 We identified *xr47*, *xr58*, and *xr60* mutations in the *kpc-1* gene through whole
109 genome sequencing. The *xr58* allele harbors a missense mutation resulting in a P440S
110 amino acid substitution at a conserved proline residue four amino acids away from the
111 catalytic serine residue toward the C-terminal(*4*). It was shown by others that *kpc-1(my24)*,

112 a different mutation in the same residue (P440L), caused a loss of function in the *kpc-1*
113 gene which resulted in defective secondary dendrite branching in PVD neurons(*22*). Thus,
114 it appears that mutations at P440 could alter KPC-1 functions moderately or severely.
115 Using the complementation test, we showed that the *kpc-1(gk8)* null mutation failed to
116 complement the *xr58* mutant phenotype in PVD neurons, further confirming that *xr58* is a
117 new *kpc-1* allele (Fig. 6d). The *xr58* mutant reveals an additional function of *kpc-1* in
118 tertiary dendrite self-avoidance as trans-heterozygous mutants (*xr58/gk8*) display the *xr58*
119 mutant phenotype of defective tertiary dendrite self-avoidance rather than defective
120 secondary dendrite branching characteristic of *gk8* (Fig. 1c, 2d). The two other *kpc-1* alleles
121 are also predicted to affect KPC-1 protein structure and function. The *xr60* allele contains
122 a missense mutation, which results in a G223S amino acid substitution in the catalytic
123 domain, whereas the *xr47* allele contains a G-to-A transition at the +1 position of intron 5,
124 which abolishes the donor splice site (Fig. 1e). Compared to the *gk8* null allele, *xr58*, *xr47*,
125 and *xr60* alleles are weaker in their phenotypic effects in PVD neurons as judged by the
126 extent of menorah coverage and trapped secondary dendrites along the primary dendrite
127 axis (Table 1). *kpc-1* mRNAs can be made from *xr58*, *xr47*, and *xr60* mutant alleles based
128 on RT-PCR amplification of respective *kpc-1* cDNAs.
129

130 **Elements in the *kpc-1* 3'UTR are required for dendrite self-avoidance**

131 The *kpc-1* genomic DNA containing the 5', coding, and 3' fragments rescued both
132 defective secondary dendrite branching and defective tertiary dendrite self-avoidance in
133 the *kpc-1(gk8)* null allele as well as defective tertiary dendrite self-avoidance in the *kpc-*
134 *1(xr58)* allele (Fig. 2 a, b). To investigate the genomic requirement of the *kpc-1* gene in

135 different steps of PVD dendrite development, we first reduced the *kpc-1* gene to the *kpc-1*
136 coding region without introns. We found that the *kpc-1* gene without introns led to a
137 complete rescue of the dendrite phenotypes in both *kpc-1(gk8)* null and *kpc-1(xr58)* alleles
138 (Fig. 2 a, b). We then further reduced the *kpc-1* promoter to a PVD cell specific promoter
139 (The F49H12.4 promoter). This *Ppvd::kpc-1::kpc-1 3'UTR* transgene remained able to
140 cause a near complete phenotypic rescue, in a manner similar to the *kpc-1* genomic DNA,
141 in both *kpc-1(gk8)* null and *kpc-1(xr58)* alleles, indicating that *kpc-1* acts cell-
142 autonomously in PVD (Fig. 2a, b, and e-h). Consistent with a cell-autonomous role of *kpc-*
143 *1* in PVD, the expression of the *kpc-1* promoter reporter was detected in PVD neurons
144 during secondary dendrite branching and tertiary dendrite self-avoidance (Fig. 2c). When
145 the *kpc-1* 3'UTR was replaced with an unrelated *unc-54* 3'UTR, the *Ppvd::kpc-1::unc-54*
146 *3'UTR* transgene was able to largely, albeit incompletely, rescue defective secondary
147 dendrite branching in the *kpc-1(gk8)* null allele (Fig. 2 a, b, d). It failed to rescue defective
148 tertiary dendrite self-avoidance in the *kpc-1(gk8)* null allele (Fig. 2 a, b, d), suggesting a
149 more stringent 3'UTR requirement for tertiary dendrite self-avoidance. In addition to
150 tertiary dendrites, some secondary dendrites displayed self-avoidance defects in these
151 transgenic animals (Fig. 2d). The same *Ppvd::kpc-1::unc-54 3'UTR* transgene was also
152 unable to rescue the defective tertiary dendrite self-avoidance in the *kpc-1(xr58)* allele (Fig.
153 2b). Increasing the concentration of the *Ppvd::kpc-1::unc-54 3'UTR* transgene from 10
154 ng/μl to 100 ng/μl did not alter this outcome. Thus, these results show that tertiary dendrite
155 self-avoidance depends on elements in the *kpc-1* 3'UTR.
156

157 **The *kpc-1* 3'UTR is required for localization of *kpc-1* mRNAs to distal primary**
158 **dendrites and higher-order tertiary dendrites in PVD neurons**

159 To directly visualize *kpc-1* mRNA distribution in PVD neurons, we utilized the
160 MS2 tagging system, which relies on the sequence-specific interaction between the MS2
161 bacteriophage RNA hairpin loops and capsid proteins. In this system, the *kpc-1* mRNA
162 containing either its own 3'UTR or a control *unc-54* 3'UTR was fused to tandem MS2
163 binding sites and co-expressed with a green fluorescent MS2 capsid fusion protein(*25*)(*26*)
164 (Fig. 3a). The green fluorescent MS2 capsid fusion protein, which is targeted to the nucleus
165 by the nuclear localization signal (Fig. 3b), binds tightly to MS2 binding sites fused to the
166 3'UTR of the *kpc-1* mRNA, allowing visualization of the *kpc-1* mRNA by MS2
167 fluorescence in PVD neurons. Using this system, we detected significant axonal and
168 dendritic signals for *kpc-1* transcripts containing its own 3'UTR (Fig. 3c, d, g). Dendritic
169 signals were preferentially distributed in the 1° and 3° dendrites (Fig. 3c, d), consistent
170 with *kpc-1*'s roles in regulating secondary dendrite branching from the 1° dendrites and
171 tertiary dendrite self-avoidance. Distribution of *kpc-1* transcripts in 3° dendrites was region
172 specific. We observed enriched localization at potential branching points and retracted
173 contact points between neighboring 3° dendrites (Fig. 3c, d). Using the mCherry reporter
174 to label PVD dendrites, we can confirm enrichment of *kpc-1* transcripts at branching points
175 and retracted contact points (Fig. 3e). In contrast, when the *kpc-1* 3'UTR was replaced with
176 an unrelated *unc-54* 3'UTR, the *kpc-1* transcripts were mainly trapped in the nucleus with
177 some perinuclear signals detected in PVD (Fig. 3f). *kpc-1* transcripts containing the *unc-*
178 *54* 3'UTR had a significantly lower chance to be transported to higher-order tertiary
179 dendrites compared to *kpc-1* transcripts containing its own 3'UTR (Fig. 3g, h). Together,

180 these results indicate that the *kpc-1* 3'UTR facilitates *kpc-1* RNA localization to distal
181 primary dendrites and higher-order tertiary dendrites, implicating local translation of *kpc-*
182 *1* in dendrites.
183
184 **The *kpc-1* 3'UTR promotes local protein synthesis in the distal segment of PVD**
185 **dendrites**
186 Our results showed that the *kpc-1* 3'UTR facilitates localization of *kpc-1* transcripts
187 to the distal primary and tertiary PVD dendrites, suggesting that the *kpc-1* 3'UTR promotes
188 local translation of transcripts it regulates. To examine whether the *kpc-1* 3'UTR can
189 promote local protein synthesis, we performed fluorescence recovery after
190 photoconversion (FRAP) of the photoconvertible Kaede protein(*27*), which was under
191 control of the *kpc-1* 3'UTR or a control *unc-54* 3'UTR. Upon photostimulation using 405
192 nm laser, Kaede proteins can be converted from green fluorescent proteins to red
193 fluorescent proteins irreversibly, allowing us to distinguish the future newly synthesized
194 green fluorescent Kaede proteins from the resident (converted) red fluorescent Kaede
195 proteins. We carried-out photoconversion at a broad region from the mid-body to the nerve
196 ring and measured newly synthesized green fluorescent Kaede proteins in a local area
197 distant away from the cell body (Fig. 4a). This design ensures that the local green
198 fluorescence signal represents newly synthesized Kaede proteins rather than resident
199 (unconverted) Kaede proteins diffused from the soma (Fig. 4a). Green fluorescence
200 recovery of Kaede proteins expressed from the *kaede::kpc-1* 3'UTR is significantly faster
201 than that from the *kaede::unc-54* 3'UTR (Fig. 4b, c), indicating that the *kpc-1* 3'UTR
202 promotes local protein synthesis in the distal segment of PVD dendrites. Using the split

203 GFP *rps-18* reporter to visualize ribosomes in PVD neurons(*28*), we detected the protein
204 synthesis machinery not only in the soma but also in secondary and tertiary dendrites (Fig.
205 4d), further supporting protein synthesis occurs in the higher order dendrites to allow for
206 proteome remodeling.
207
208 **Identification and characterization of secondary structural motifs in the *kpc-1* 3'UTR**
209 **required for tertiary dendrite self-avoidance**
210 Many studies have shown that specific elements in 5′ or 3′ untranslated regions
211 (UTRs) of mRNA regulate mRNA stability, splicing, translation and localization(*29*).
212 microRNAs regulate mRNA translation and stability by binding to complementary
213 sequences in the 3′UTR(*30*). Other types of elements in the 3'UTR can function in either
214 a sequence- or secondary structure-specific manner. For example, one of the earliest
215 identified localization elements was discovered from the chick β-actin mRNA. The
216 "zipcode" in the 3′UTR of β-actin mRNA consists of 54 nucleotides that contain tandem
217 repeats of the conserved hexanucleotide motif ACACCC and form a stem-loop structure
218 recognized by the Zipcode Binding Proteins (ZBPs) to regulate the localization and
219 translation of β-actin mRNA(*31*, *32*). In yeast, the cis-acting sequences that mediate ASH1
220 mRNA targeting to the bud tip provide another example of repetitive clustering and
221 synergistic action of localization elements. Four localization elements in ASH1 mRNA
222 were all predicted to form stem-loop structures, and each element on its own is able to
223 localize mRNAs, but the presence of four elements together increases the efficiency of
224 localization(*33–35*). In Aplysia sensory-motor neurons, cis-elements in the 3′ UTR of the
225 neurotransmitter sensorin mRNA control the transport of sensorin mRNAs from soma to

226 neurite(*36*). In mice, conditional deletion of an axon-localizing cis-element in the 3′UTR
227 of importin β1 mRNAs in sensory neurons caused selective depletion of importin β1
228 mRNAs and proteins in axons, without affecting cell body levels or nuclear functions,
229 suggesting that local translation of importin β1 mRNAs in axons enables separation of
230 axonal and nuclear transport functions of importins, and is required for efficient retrograde
231 signaling in injured axon(*37*).

232 In *C. elegans*, it was previously reported that the *cebp-1* 3'UTR is required for the
233 localization of *cebp-1* mRNAs to discrete locations in touch axons, which can be translated
234 into proteins locally(*38*). What is unclear is whether those discrete locations represent
235 synapses in touch axons. In addition, a putative stem-loop secondary structure was
236 identified in the *cebp-1* 3'UTR that inhibits *cebp-1* mRNA stability or its translation(*39*).
237 Thus, the *cebp-1* 3'UTR appears to have both positive and negative impacts on *cebp-1* gene
238 expression.

239 Secondary structural motifs derived from the alignment of *kpc-1* 3'UTRs from 4
240 closely-related nematode species, including *C. elegans* (Supplementary Fig. 3), as well as
241 individual Turbofold II-predicted secondary structures(*40*), revealed that two stem-loop
242 structural motifs (SLS1 and SLS2) are conserved in the 3' UTR of all *kpc-1* homologs (Fig.
243 5a). The *kpc-1* transgene with its 3'UTR being replaced by a control *unc-54* 3'UTR lost
244 the ability to rescue tertiary dendrite self-avoidance defects in the *kpc-1(gk8)* null allele
245 (Fig. 5f). Deletion analysis showed that SLS2 but not SLS1 is required for the *kpc-1* 3'UTR
246 to mediate tertiary dendrite self-avoidance since *ΔSLS2* but not *ΔSLS1* in the *kpc-1* 3'UTR
247 abolished the ability of the *kpc-1* transgene to rescue tertiary dendrite self-avoidance
248 defects in the *kpc-1(gk8)* null allele (Fig. 5f). The *kpc-1* transgene with mutations that

249 disrupt base-pairing in the stem region of SLS2 in the 3'UTR exhibited significantly more
250 contacts between sibling tertiary dendrites (indicating losing self-avoidance functions; Fig.
251 5c, f) whereas the *kpc-1* transgene with reciprocal mutations that preserve base-pairing in
252 the stem region of SLS2 in the 3'UTR did not cause more contacts between sibling tertiary
253 dendrites (indicating maintaining self-avoidance functions; Fig. 5d, f).

254 All the *kpc-1* transgenes tested here partially rescued secondary dendrite branching
255 defects in the *kpc-1(gk8)* null allele, suggesting that the modifications we introduced to the
256 transgenes, including the 3'UTR replacement, deletions, and mutations, did not result in
257 degradation of the *kpc-1* transcripts (Fig. 5e). Levels of the *kpc-1* RNA expressed from
258 various transgenes in *kpc-1(gk8)* mutants were analyzed by RT-PCR. All *kpc-1* 3'UTR
259 modifications were made from the PF49H12.4::*kpc-1s*::*kpc-1* 3'UTR construct, where only
260 the short-isoform *kpc-1s* RNA would be generated. We found that the *kpc-1* RNA
261 expression levels are comparable among different *kpc-1* transgenes (Supplementary Fig.
262 4), indicating that modifications we introduced to the *kpc-1* 3'UTR did not affect the *kpc-*
263 *1* RNA stability. Furthermore, even though the level of the endogenous *kpc-1* RNA in wild-
264 type animals (containing both long and short isoforms) is lower, it promotes dendrite self-
265 avoidance better than a higher level of the short-isoform (*kpc-1s* RNA) expressed from
266 various transgenes in PVD neurons of *kpc-1(gk8)* mutants (Supplementary Fig. 4).
267 Together, our results have identified an important secondary structural motif in the *kpc-1*
268 3'UTR required for tertiary dendrite self-avoidance.

269 To validate the role of the *kpc-1* 3'UTR secondary structural motif SLS2 in PVD
270 dendrite branching and self-avoidance, we applied the CRISPR-Cas9 engineering to
271 generate mutations in the *kpc-1* 3'UTR. Due to the AT-rich sequence in the region

272 surrounding the SLS2 site, only suboptimal sgRNAs with low target selectivity could be
273 designed, which prevented generation of specific SLS2 mutations. A more distal but
274 selective sgRNA was subsequently designed to generate a 296 base-pair deletion that
275 includes the SLS2 site. Although transgene experiment using *kpc-1(gk8)* mutants carrying
276 the *Ppvd::kpc-1::kpc-1* 3'UTR transgene with mutated SLS2 base pairing demonstrated an
277 importance role of SLS2 in dendrite self-avoidance, the CRISPR-Cas9 engineered *kpc-*
278 *1(xr82) [SLS2 deleted]* mutant allele only showed a weak tertiary dendrite self-avoidance
279 defect (Supplementary Fig. 5a). The mild phenotypic effects of the *kpc-1(xr82)* mutant
280 allele were inadvertently caused by the creation of a new stem-loop structure that likely
281 substitutes the SLS2's function. Although the *xr58* or *xr82 [SLS2 deleted]* allele alone did
282 not cause a severe self-avoidance defect, introducing the *xr84 [SLS2 deleted]* allele into
283 the *kpc-1(xr58)* background collectively caused significantly more secondary dendrite
284 branching defects compared to wild-type (Supplementary Fig. 5b). Taken together, our
285 results indicate that both the *kpc-1* coding region and its 3'UTR are required for PVD
286 dendrite patterning.
287
288 **KPC-1 down-regulates DMA-1 receptors on PVD tertiary dendrites**
289 While the number of tertiary dendrites was significantly reduced in *sax-7*, *mnr-1*,
290 *lect-2*, or *dma-1* mutants, it was significantly increased in *kpc-1(xr58)* mutants(*16*, *17*, *19–*
291 *21*) (Fig. 1c). These results suggested that *kpc-1* likely antagonizes the *sax-7/mnr-1/lect-*
292 *2/dma-1* signaling pathway. Double mutant analyses revealed that *sax-7*, *mnr-1*, *lect-2*, and
293 *dma-1* mutations completely suppressed the *kpc-1(xr58)* mutant phenotype of excessive
294 tertiary dendrites, indicating that the *kpc-1* mutant effect depends on the *sax-7/mnr-1/lect-*

295 *2/dma-1* signaling pathway. The *kpc-1(gk8)* null allele seems to have a phenotype very
296 similar to the *sax-7*, *mnr-1*, *lect-2*, and *dma-1* mutants(*16*, *17*, *19–21*) (Fig. 2d, e). However,
297 closer examination of the *kpc-1(gk8)* null mutant phenotype revealed that defective
298 secondary dendrite extension to sublateral longitudinal stripes is caused by a failure of
299 secondary dendrites branching out(*4*), a phenotype that is clearly different from the less
300 secondary dendrite outgrowth in *sax-7*, *mnr-1*, *lect-2*, and *dma-1* mutants. Double mutant
301 analyses between the *kpc-1(gk8)* null allele and *sax-7*, *mnr-1*, and *dma-1* mutations have
302 been reported in a recent paper(*4*), which also supported that *kpc-1* antagonizes the *sax-*
303 *7*/*mnr-1*/*dma-1* signaling pathway in PVD neurons. *dma-1*, like *kpc-1*, encodes a
304 transmembrane protein and acts cell-autonomously in PVD neurons(*4*, *19*). Thus, DMA-1
305 could be a potential KPC-1 target in regulating PVD tertiary dendrite self-avoidance.
306 Supporting this possibility, endogenous DMA-1 protein levels on PVD tertiary dendrites
307 were up-regulated in *kpc-1* mutants, suggesting that KPC-1 normally down-regulates
308 DMA-1 on PVD tertiary dendrites (Fig. 6 a, b). In addition, the *kpc-1(xr47)* mutant allele,
309 which showed a greater increase in the number of overlapped tertiary dendrites compared
310 to the *kpc-1(xr58)* mutant allele (Fig. 6c), caused a greater up-regulation of the DMA-1
311 protein level on PVD tertiary dendrites than the *kpc-1(xr58)* mutant allele (Fig. 6 a, b). A
312 recent paper reported a different phenotypic effect of *kpc-1* mutations in PVD neurons
313 where *kpc-1* mutations caused excessive DMA-1 receptors on secondary dendrites, which
314 resulted in secondary dendrites trapped in the primary dendrite zone where a high level of
315 the cognate ligand SAX-7/L1CAM is present(*4*).
316
317 **The *kpc-1-dma-1* regulatory circuit promotes dendrite self-avoidance**

318 To further strengthen the conclusion of a *kpc-1-dma-1* regulatory circuit in
319 promoting PVD dendrite self-avoidance, we tested whether *dma-1* over-expression (OE)
320 mimics the *kpc-1* mutation in its phenotypic effect on PVD dendrites. *dma-1* OE displayed
321 a tertiary dendrite self-avoidance defect similar to that exhibited by the *kpc-1(xr58)* mutant
322 allele (Fig. 7 a, b). In addition, *dma-1* OE caused a secondary dendrite branching phenotype
323 (Fig. 7d), which was further enhanced by the *kpc-1(xr58)* mutation. In contrast, *kpc-1* OE
324 suppressed the secondary dendrite branching phenotype in *dma-1* OE animals (Fig. 7c-f).
325 While fewer *kpc-1* OE*; dma-1* OE animals displayed a secondary dendrite branching
326 phenotype, most still exhibited a weak tertiary dendrite self-avoidance defect, which was
327 milder than *dma-1* OE or *kpc-1(xr58)* alone. Thus, a weaker *kpc-1-dma-1* regulatory circuit
328 causes tertiary dendrite self-avoidance defects whereas a further reduced *kpc-1-dma-1*
329 regulatory circuit results in secondary dendrite branching defects. Indeed, the mild *kpc-*
330 *1(xr58)* mutant allele preferentially affects tertiary dendrite self-avoidance rather than
331 secondary dendrite branching. Together, our results support a model in which locally
332 expressed KPC-1 down-regulates DMA-1 receptors on PVD dendrites to promote dendrite
333 branching and self-avoidance (Fig. 7k).

334 We have made different versions of KPC-1::dzGFP^{myr} and KPC-1::GFP fusion
335 proteins, both wild-type and mutant forms that disrupted the KPC-1 self-cleavage site.
336 However, we were unable to detect any fluorescence signal beyond the PVD cell body
337 (unpublished), suggesting that KPC-1 proteins have very short half-life in PVD dendrites.
338 Due to this technical limitation, we cannot determine whether KPC-1 proteins are
339 synthesized locally in tertiary dendrites. Nor can we address whether the KPC-1 protein
340 and its substrate DMA-1 specifically colocate to higher order dendrites. As an alternative

341 approach, we superimposed the image of dendritic signals for *kpc-1* transcripts with the
342 image of dendritic signals for DMA-1 proteins. We found that they did not show
343 overlapping distribution pattern (Fig. 7 g, h). Instead, adjacent sites of expression can be
344 detected for *kpc-1* mRNAs and DMA-1 proteins (Fig. 7 g, h), consistent with down-
345 regulation of DMA-1 by KPC-1 at specific sites.

346 The tertiary dendrite self-avoidance defect could result from either excessive
347 dendrite growth ability that overcomes a self-avoidance mechanism or insufficient self-
348 avoidance. To distinguish between these two possibilities, we performed laser dendritomy
349 in PVD neurons at the early L4 stage when tertiary dendrites underwent self-avoidance and
350 assessed the dendrite growth ability 24h after surgery. Dendrites were cut at the primary
351 branch 20 μm anterior to the cell body such that the entire anterior dendrite arbor was
352 disconnected from the cell body after surgery. We found that PVD dendrite growth ability
353 was not significantly enhanced in *kpc-1(xr58)* mutants compared to wild-type animals (Fig.
354 7i). This result indicated that the dendrite self-avoidance defect in *kpc-1(xr58)* mutants
355 cannot be attributed to excessive dendrite growth ability.

356 In contrast, over-expression of *kpc-1* significantly increased the distance (gap)
357 between neighboring tertiary dendrites (Fig. 7 c, j). This result suggested that *kpc-1* either
358 limited tertiary branch outgrowth or promoted tertiary dendrite self-avoidance. Time-lapse
359 imaging revealed that neighboring tertiary dendrites in *kpc-1* over-expression animals
360 actually contacted at first and retracted subsequently, suggesting that *kpc-1* over-
361 expression did not limit tertiary branch outgrowth. Together, these results support that *kpc-*
362 *1* promotes dendrite self-avoidance rather than limiting dendrite outgrowth.

363

364 **Defective PVD dendrite arborization causes reduced male mating efficiency**

365 The mechanical sensation is known to regulate animal locomotion and posture
366 during male mating behavior(*41*)·(*42*). PVD neurons are known mechanosensors but
367 whether they are involved in male mating behavior is not known. Mature PVD dendrite
368 arbors display a sensory network that innervates the skin area outside of the head region.
369 We characterized PVD dendrites in *kpc-1(xr58)* mutant males and found that *kpc-1(xr58)*
370 mutant males also displayed dendrite self-avoidance defects and reduced sensory coverage
371 of skin by PVD dendrite arbors (Fig. 8a-c). To determine whether fully extended dendrite
372 arbors of PVD neurons are crucial for male mating behavior, we assessed the mating
373 efficiency of *kpc-1* mutant males. The *kpc-1(xr58)* mutants males showed reduced
374 reproductive efficiencies (Fig. 8d), suggesting that PVD neurons are involved in the male
375 courtship process. The male mating process begins with males responding to the
376 hermaphrodite contact, turning around the hermaphrodite's head and tail, until the vulva is
377 located. We found that *kpc-1(xr58)* mutant males have no problem responding to
378 hermaphrodite contact (Fig. 8e) but are required to make more turns to mate with
379 hermaphrodite successfully (Fig. 8f). Therefore, PVD neurons likely coordinate diverse
380 behavioral motifs in reproductive behavior. These results suggest that male mating
381 behavior requires the mechanosensory inputs from PVD neurons to ensure sufficient
382 mating motor patterns.

383 **Discussion**

384 Our results support a model where locally synthesized KPC-1 at branching points and
385 contact points between sibling dendrites down-regulates DMA-1 receptors to promote
386 dendrite branching and self-avoidance (Fig. 7k). A recent paper showed that KPC-1
387 targeted DMA-1 to endosomes for degradation in PVD neurons(*4*). It is likely that a similar
388 mechanism is utilized in a site-specific manner for secondary dendrite branching(*4*) and
389 tertiary dendrite self-avoidance. KPC-1 encodes a proprotein convertase subtilisin/kexin
390 (PCSK). At a functional level, there are two types of mammalian PCSKs. PCSK3/furin
391 activates substrates by cleavage of precursor proteins, such as TGF-β, whereas PCSK9
392 inactivates substrates by induced degradation of proteins, such as LDL receptors(*43–46*).
393 Our results indicate that KPC-1 is more closely related to PCSK9 at a functional level in
394 its inactivation of DMA-1. It has been shown that PCSK9 is expressed in the vertebrate
395 CNS, including the cerebellum, and is important for CNS development(*47*). However, it
396 remains to be seen whether PCSK9 plays a similar role to KPC-1 in dendrite branching and
397 self-avoidance by down-regulating dendrite receptors.

398 It is necessary that the level of DMA-1 receptors on tertiary dendrites is tightly
399 controlled during dendrite outgrowth and self-avoidance (Fig. 7k). For example, the DMA-
400 1 receptor level should be high on tertiary dendrites during dendrite outgrowth. However,
401 the DMA-1 receptor level needs to be down-regulated upon contact between sibling tertiary
402 dendrites, resulting in dendrite retraction (self-avoidance). An important question that
403 remains to be addressed in the future is how the KPC-1 activity is dynamically controlled
404 to regulate corresponding DMA-1 levels. There are two possible regulatory mechanisms
405 that could be responsible: expression versus activation of KPC-1 at the contact points

406 between sibling dendrites. Our observation of the enrichment of *kpc-1* transcripts at the
407 contact points appears to support the former case (Fig. 3e). However, it is not known how
408 *kpc-1* transcripts are targeted to contact points and whether contact-triggered RNA
409 transport is responsible.

410 Although our results demonstrate the important role of the *kpc-1* 3'UTR in
411 promoting *kpc-1* mRNA transport to the PVD higher order dendrites, questions remain on
412 how the 3'UTR elements interact with the RNA transport system. It was recently reported
413 that 12 conserved RNA-binding protein (RBP)-encoding genes are involved in PVD
414 dendrite development in *C. elegans*(*48*). Among them, loss of function in *cgh-1* and *cpb-3*
415 resulted in an increase in the number of tertiary dendrite branches. The phenotype of
416 increased number of tertiary dendrite branches is also shared by *kpc-1(xr58)* mutants (Fig.
417 1c). Like *kpc-1*, *cgh-1* and *cpb-3* act cell-autonomously in PVD neurons to control dendrite
418 development. Also, like *kpc-1* transcripts, CGH-1 and CPB-3 proteins are enriched in PVD
419 dendrites, raising the possibility that CGH-1 and CPB-3 may regulate the *kpc-1* function
420 in dendrites by binding to the 3'UTR of *kpc-1* mRNAs, a possibility awaiting to be
421 explored. A Schizophrenia-associated genetic variant in the 3'UTR of the human furin
422 gene, a *kpc-1* homologous gene, was recently shown to result in downregulation of furin
423 expression by acquiring a miR-338-3p binding site, leading to reduced BDNF production.
424 It remains to be seen whether this human furin 3'UTR genetic variant disrupts transport
425 and local translation of the furin mRNA in dendrites and whether it affects dendrite
426 patterning in Schizophrenia-causing neurons(*1*, *49*).
427

428 **Experimental Procedures**

429 **Strains and plasmids**

430 *C. elegans* strains were cultured using standard methods(*50*). All strains were grown at
431 20°C. Standard protocol was used for the plasmid constructions. Strains and plasmids are
432 listed in Supplementary Tables S1 and S2.

433

434 **Isolation of *kpc-1* alleles from the genetic screen**

435 A forward genetic screen was conducted as previously described. Wild type worms with
436 *xrIs37* marker were treated with EMS. F1 progenies were transferred to single plates, and
437 F2 progenies were screened for profoundly affected dendrite self-avoidance defect. Using
438 a Zeiss fluorescence dissecting microscope. The *kpc-1(xr47)*, *kpc-1(xr58)*, and *kpc-1(xr60)*
439 mutations were identified from a screen of 9,500 genomes.

440

441 **Transgenic animals**

442 Germline transformation of *C. elegans* was performed using standard techniques(*51*). For
443 example, the *Pkpc-1(5K)::kpc-1* transgene was injected at 10 ng/ml along with the
444 coinjection marker *ofm-1::rfp* at 50 ng/µl. Transgenic lines were maintained by following
445 the *ofm-1::rfp* fluorescence.

446

447 **Tertiary branch avoidance index (TBAI)**

448 TBAI was calculated by dividing the number of visible gaps between tertiary branches by
449 the number of menorahs. A menorah-like structure is composed of a collection of 2°
450 ("stem"), 3° ("base") and 4° ("candles") branches. In the case where discrete menorahs

451 cannot be easily differentiated due to self-avoidance defects, we counted each menorah as
452 a single 2° ("stem") branch that extended 3° ("base") branches.
453
454 **Scatter plots of quaternary dendrite termini**
455 To map out quaternary dendrite termini, we used a set of customized MatLab scripts
456 (MatLAB, Mathworks, Natick, MA) to effectively unroll the worm's cylindrical surface,
457 quantifying anterior-posterior distances using the coordinate parallel to the body centerline
458 and dorsal-ventral distances along the cylindrical surface. In order to consolidate data from
459 different worms, all scatter plots are scaled to each worm's circumference. In each scatter
460 plot, the top line indicates the dorsal nerve cord, the bottom line indicates the ventral nerve
461 cord, and the wild-type morphology of the PVD primary dendrite and axon is drawn in
462 green. The distance between the top and bottom lines corresponds to 1/2 of total worm
463 circumference, and the horizontal axis shows a portion of body length equivalent to
464 approximately 3 circumferences.
465
466 **Molecular cloning**
467 All constructs generated for this study are summarized in Table S2. Sequence variants of
468 the *kpc-1* 3'UTR were verified by sequencing.
469
470 **CRISPR-Cas-9 genome editing**
471 To generate deletion of the SLS2 region in the *kpc-1* 3'UTR, we used the Co-CRISPR *dpy-*
472 *10(cn64)* as a screening method(*52*). Worms were injected with Cas9_sgRNA plasmid and

473 single-stranded oligonucleotide donor (IDT). Both *xr82* and *xr84* SLS2 deletion alleles
474 were confirmed by sequencing.
475
476 **Laser dendritomy**
477 For the femtosecond laser surgery, we used a cavity-dumped Ti:sapphire laser
478 oscillator(*53*, *54*) to generate laser pulses ~100 fs in duration and 200 kHz in repetition
479 rate. The laser pulses were tightly-focused onto targeted primary dendrites using a Nikon
480 100x, 1.4 NA oil-immersion objective. The vaporization threshold corresponds to pulse
481 energies of 5-15 nJ. Successful laser dendritomy was confirmed by visualizing the targeted
482 area immediately after surgery. Dendrites were cut at the primary branch 50 μm anterior
483 to the cell body in the early L4 stage when tertiary dendrites undergo self-avoidance. 1°,
484 2°, 3°, and 4° dendrites in the anterior dendrite arbor were disconnected from the cell body
485 after primary dendritomy. Newly regenerated dendrites can be easily differentiated from
486 the old dendrites 24 hr after surgery due to difference in the fluorescence intensity of the
487 *Pser-2::GFP* dendrite marker.
488
489 **Imaging and quantifying dendrite arbors**
490 The morphology of neuronal cell bodies and dendrites was based on high-magnification Z-
491 stacks using a Zeiss 60x, 1.4 NA oil-immersion objective. For laser dendritomy, we
492 mounted individual animals on 2% agar pads and anaesthetized them with 3 mM sodium
493 azide, the lowest possible concentration to keep adult animals immobilized. Laser
494 dendritomy was performed and worms were recovered within 10 minutes of sodium azide
495 treatment. Recovered worms were placed on fresh plates with bacterial foods and imaged

496 24 hours after dendritomy using a Hamamatsu ORCA AG camera. For imaging and
497 quantifying uninjured dendrite arbors, young adult animals were mounted on 2% agar pads
498 and anaesthetized with 20 mM sodium azide.

499 The dendrite length of regenerating neurons was quantified 24 hours after surgery.
500 Dendrite lengths were calculated as the actual contour length between the injury site and
501 dendrite termini measured along the cylindrical surface of each worm, by tracing dendrites
502 through a 3-dimensional image stack. P values for the length measurements were calculated
503 using a student's t-Test**.**

504

505 **Fluorescence microscopy**

506 Worms were mounted on 2% agarose pad and anaesthetized with 20 mM sodium azide
507 solution. Images were acquired using a 40x, 1.4 NA objective on a Zeiss Axio Imager M2
508 microscope with a Hamamatsu ORCA-Flash4.0 LT+ camera. Images were processed by z-
509 stack projections.

510

511 **Fluorescence recovery after photoconversion**

512 Worms were mounted on 2% agarose pad and anaesthetized with 7.5 mM tetramisole.
513 Photoconversion of Kaede was performed under 405 nm laser on the region of interest
514 (ROI). Fluorescence quantification of ROI intensity was measured every 5 seconds over 6
515 minutes following photoconversion (Zeiss Imaging Browser). At each time point,
516 percentage green fluorescence signal recovery was determined by $(F_n-F_0)/(F_p-F_0)$, where
517 F_n = fluorescence intensity n seconds after photoconversion; F_0 = fluorescence intensity
518 immediately after photoconversion; F_p = fluorescence intensity right before

519 photoconversion. All images were taken in live animals using a 40x, 1.3 NA objective and
520 488 nm and 561 nm laser on a Zeiss LSM 880 confocal microscope.
521
522 **Male mating behavior assays**
523 Male mating behavioral assays were conducted using standard methods(*55*). Reproductive
524 efficiencies were conducted by placing six males with seven hermaphrodite carrying *unc-*
525 *36(e251)* recessive marker and results were calculated by the number of cross-progeny over
526 total number progeny. Three repeats were conducted on separate days. Number of
527 hermaphrodites contacted before mating initiation were counted within 5 minutes of male
528 first contacted the hermaphrodites. Total number of turns around hermaphrodites during
529 mating were counted before males successfully identify the vulva.
530
531 **Statistics**
532 Average data of dendrite number, dendrite length, TBAI, receptive field index, length ratio
533 of receptive field, and reporter expression intensity are presented as means ± SEM. Data
534 of % PVD neurons with secondary dendrite branching defects, defective dendrite self-
535 avoidance, and dendritic signals are presented as proportions ± SEP. Statistical analyses
536 were carried out by Student's *t*-tests, two-proportion *Z*-tests, or one-way ANOVA with
537 Tukey's or Dunnett's tests using GraphPad Prism 7.0 or the Primer of Biostatistics
538 software.
539
540
541

542 **Author Contributions**

543 M.S. conceived, designed, performed, and analyzed experiments, made constructs, and
544 drafted the article related to figures 4, 5, 8, and S3-S5. Y.Z. conceived, designed,
545 performed, and analyzed experiments, and made constructs. T.F. performed genetic
546 screens, identified dendrite self-avoidance mutants, determined receptive field index and
547 length ratio of receptive field in PVD dendrite arbors, and drew scatter plots of 4° dendrite
548 termini using MATLAB. N.Z. imaged and quantified green fluorescent MS2 capsid
549 proteins in PVD dendrites. E.K. performed male mating behavioral assays and analyzed
550 results. C.F.C. conceived, designed, and analyzed experiments. C.C. conceived, designed,
551 analyzed and interpreted data, and drafted the article.

552

553

554 **Acknowledgments**

555 This work was funded by grants from the March of Dimes Foundation (C.C.), the Whitehall
556 Foundation Research Award (C.C.), the National Science Foundation (IOS-1455758 to
557 C.C.), and the National Institute of General Medical Sciences of the National Institutes of
558 Health (R01GM111320 to C.C.). We thank Oliver Hobert lab for Whole Genome
559 Sequencing, Daniel J. Dickinson and Bob Goldstein for providing reagents and CRISPR
560 protocols, Kana Hamada for confocal imaging protocols, Ryan Weihsiang Lin for imaging
561 analysis, Seema Sheoran for unpublished observation, Evguenia Ivakhnitskaia for critical
562 reading the manuscript, Hui Chiu for critical reading the manuscript, providing critical
563 initial data, and making main figures, Kang Shen for the *dma-1(wy1246) [dma-1::GFP]*

564 allele, the *Caenorhabditis* Genetics Center for the *kpc-1(gk8)* strain, and the WormBase
565 for readily accessible information.
566

567 **References**

568 1. N. Schrode, S.-M. Ho, K. Yamamuro, A. Dobbyn, L. Huckins, M. R. Matos, E.
569 Cheng, P. J. M. Deans, E. Flaherty, N. Barretto, A. Topol, K. Alganem, S. Abadali,
570 J. Gregory, E. Hoelzli, H. Phatnani, V. Singh, D. Girish, B. Aronow, R.
571 Mccullumsmith, G. E. Hoffman, E. A. Stahl, H. Morishita, P. Sklar, K. J. Brennand,
572 Synergistic effects of common schizophrenia risk variants. *Nat. Genet.* **51**, 1475–
573 1485 (2019).

574 2. J. C. Way, M. Chalfie, The mec-3 gene of Caenorhabditis elegans requires its own
575 product for maintained expression and is expressed in three neuronal cell types.
576 *Genes Dev.* **3**, 1823–1833 (1989).

577 3. N. Suzuki, Y. Zou, H. Sun, K. Eichel, M. Shao, M. Shih, K. Shen, C. Chang, Two
578 intrinsic timing mechanisms set start and end times for dendritic arborization of a
579 nociceptive neuron. *Proc. Natl. Acad. Sci.* **119**, e2210053119 (2022).

580 4. X. Dong, H. Chiu, Y. J. Park, W. Zou, Y. Zou, E. Özkan, C. Chang, K. Shen, Precise
581 regulation of the guidance receptor DMA-1 by KPC-1/Furin instructs dendritic
582 branching decisions. *eLife* **5**, e11008 (2016).

583 5. C. J. Smith, J. D. Watson, W. C. Spencer, T. O'Brien, B. Cha, A. Albeg, M. Treinin,
584 D. M. Miller, Time-lapse imaging and cell-specific expression profiling reveal
585 dynamic branching and molecular determinants of a multi-dendritic nociceptor in C.
586 elegans. *Dev. Biol.* **345**, 18–33 (2010).

587 6. C. J. Smith, J. D. Watson, M. K. VanHoven, D. A. Colón-Ramos, D. M. Miller,
588 Netrin (UNC-6) mediates dendritic self-avoidance. *Nat. Neurosci.* **15**, 731–737
589 (2012).

590 7. A. P. Kramer, J. Y. Kuwada, Formation of the receptive fields of leech
591 mechanosensory neurons during embryonic development. *J. Neurosci. Off. J. Soc.*
592 *Neurosci.* **3**, 2474–2486 (1983).

593 8. A. P. Kramer, G. S. Stent, Developmental arborization of sensory neurons in the
594 leech Haementeria ghilianii. II. Experimentally induced variations in the branching
595 pattern. *J. Neurosci. Off. J. Soc. Neurosci.* **5**, 768–775 (1985).

596 9. X.-L. Zhan, J. C. Clemens, G. Neves, D. Hattori, J. J. Flanagan, T. Hummel, M. L.
597 Vasconcelos, A. Chess, S. L. Zipursky, Analysis of Dscam diversity in regulating
598 axon guidance in Drosophila mushroom bodies. *Neuron* **43**, 673–686 (2004).

599 10. W. M. Wojtowicz, J. J. Flanagan, S. S. Millard, S. L. Zipursky, J. C. Clemens,
600 Alternative splicing of Drosophila Dscam generates axon guidance receptors that
601 exhibit isoform-specific homophilic binding. *Cell* **118**, 619–633 (2004).

602 11. M. E. Hughes, R. Bortnick, A. Tsubouchi, P. Bäumer, M. Kondo, T. Uemura, D.
603 Schmucker, Homophilic Dscam interactions control complex dendrite
604 morphogenesis. *Neuron* **54**, 417–427 (2007).

605 12. B. J. Matthews, M. E. Kim, J. J. Flanagan, D. Hattori, J. C. Clemens, S. L. Zipursky,
606 W. B. Grueber, Dendrite self-avoidance is controlled by Dscam. *Cell* **129**, 593–604
607 (2007).

608 13. P. Soba, S. Zhu, K. Emoto, S. Younger, S.-J. Yang, H.-H. Yu, T. Lee, L. Y. Jan, Y.-
609 N. Jan, Drosophila sensory neurons require Dscam for dendritic self-avoidance and
610 proper dendritic field organization. *Neuron* **54**, 403–416 (2007).

611 14. C.-P. Liao, H. Li, H.-H. Lee, C.-T. Chien, C.-L. Pan, Cell-Autonomous Regulation of
612 Dendrite Self-Avoidance by the Wnt Secretory Factor MIG-14/Wntless. *Neuron* **98**,
613 320-334.e6 (2018).

614 15. H.-W. Hsu, C.-P. Liao, Y.-C. Chiang, R.-T. Syu, C.-L. Pan, Caenorhabditis elegans
615 Flamingo FMI-1 controls dendrite self-avoidance through F-actin assembly. *Dev.*
616 *Camb. Engl.* **147**, dev179168 (2020).

617 16. X. Dong, O. W. Liu, A. S. Howell, K. Shen, An extracellular adhesion molecule
618 complex patterns dendritic branching and morphogenesis. *Cell* **155**, 296–307
619 (2013).

620 17. Y. Salzberg, C. A. Díaz-Balzac, N. J. Ramirez-Suarez, M. Attreed, E. Tecle, M.
621 Desbois, Z. Kaprielian, H. E. Bülow, Skin-derived cues control arborization of
622 sensory dendrites in Caenorhabditis elegans. *Cell* **155**, 308–320 (2013).

623 18. A. Albeg, C. J. Smith, M. Chatzigeorgiou, D. G. Feitelson, D. H. Hall, W. R. Schafer,
624 D. M. Miller, M. Treinin, C. elegans multi-dendritic sensory neurons: morphology
625 and function. *Mol. Cell. Neurosci.* **46**, 308–317 (2011).

626 19. O. W. Liu, K. Shen, The transmembrane LRR protein DMA-1 promotes dendrite
627 branching and growth in C. elegans. *Nat. Neurosci.* **15**, 57–63 (2011).

628 20. W. Zou, A. Shen, X. Dong, M. Tugizova, Y. K. Xiang, K. Shen, A multi-protein
629 receptor-ligand complex underlies combinatorial dendrite guidance choices in C.
630 elegans. *eLife* **5**, e18345 (2016).

631 21. C. A. Díaz-Balzac, M. Rahman, M. I. Lázaro-Peña, L. A. Martin Hernandez, Y.
632 Salzberg, C. Aguirre-Chen, Z. Kaprielian, H. E. Bülow, Muscle- and Skin-Derived
633 Cues Jointly Orchestrate Patterning of Somatosensory Dendrites. *Curr. Biol. CB* **26**,
634 2379–2387 (2016).

635 22. N. E. Schroeder, R. J. Androwski, A. Rashid, H. Lee, J. Lee, M. M. Barr, Dauer-
636 specific dendrite arborization in C. elegans is regulated by KPC-1/Furin. *Curr. Biol.*
637 *CB* **23**, 1527–1535 (2013).

638 23. Y. Salzberg, N. J. Ramirez-Suarez, H. E. Bülow, The proprotein convertase KPC-
639 1/furin controls branching and self-avoidance of sensory dendrites in Caenorhabditis
640 elegans. *PLoS Genet.* **10**, e1004657 (2014).

641 24. S. L. Zipursky, W. B. Grueber, The molecular basis of self-avoidance. *Annu. Rev.*
642 *Neurosci.* **36**, 547–568 (2013).

643 25. E. Bertrand, P. Chartrand, M. Schaefer, S. M. Shenoy, R. H. Singer, R. M. Long,
644 Localization of ASH1 mRNA Particles in Living Yeast. *Mol. Cell* **2**, 437–445
645 (1998).

646 26. A. Aizer, A. Kalo, P. Kafri, A. Shraga, R. Ben-Yishay, A. Jacob, N. Kinor, Y. Shav-
647 Tal, Quantifying mRNA targeting to P-bodies in living human cells reveals their
648 dual role in mRNA decay and storage. *J. Cell Sci.* **127**, 4443–4456 (2014).

649 27. R. Ando, H. Hama, M. Yamamoto-Hino, H. Mizuno, A. Miyawaki, An optical
650 marker based on the UV-induced green-to-red photoconversion of a fluorescent
651 protein. *Proc. Natl. Acad. Sci. U. S. A.* **99**, 12651–12656 (2002).

652 28. K. Noma, A. Goncharov, M. H. Ellisman, Y. Jin, Microtubule-dependent ribosome
653 localization in C. elegans neurons. *eLife* **6**, e26376 (2017).

654 29. F. Mignone, C. Gissi, S. Liuni, G. Pesole, Untranslated regions of mRNAs. *Genome*
655 *Biol.* **3**, REVIEWS0004 (2002).

656 30. M. R. Fabian, N. Sonenberg, W. Filipowicz, Regulation of mRNA translation and
657 stability by microRNAs. *Annu. Rev. Biochem.* **79**, 351–379 (2010).

658 31. E. H. Kislauskis, X. Zhu, R. H. Singer, Sequences responsible for intracellular
659 localization of beta-actin messenger RNA also affect cell phenotype. *J. Cell Biol.*
660 **127**, 441–451 (1994).

661 32. A. F. Ross, Y. Oleynikov, E. H. Kislauskis, K. L. Taneja, R. H. Singer,
662 Characterization of a beta-actin mRNA zipcode-binding protein. *Mol. Cell. Biol.* **17**,
663 2158–2165 (1997).

664 33. P. Chartrand, X. H. Meng, R. H. Singer, R. M. Long, Structural elements required for
665 the localization of ASH1 mRNA and of a green fluorescent protein reporter particle
666 in vivo. *Curr. Biol. CB* **9**, 333–336 (1999).

667 34. I. Gonzalez, S. B. Buonomo, K. Nasmyth, U. von Ahsen, ASH1 mRNA localization
668 in yeast involves multiple secondary structural elements and Ash1 protein
669 translation. *Curr. Biol. CB* **9**, 337–340 (1999).

670 35. P. Chartrand, X. H. Meng, S. Huttelmaier, D. Donato, R. H. Singer, Asymmetric
671 sorting of ash1p in yeast results from inhibition of translation by localization
672 elements in the mRNA. *Mol. Cell* **10**, 1319–1330 (2002).

673 36. E. J. Meer, D. O. Wang, S. Kim, I. Barr, F. Guo, K. C. Martin, Identification of a cis-
674 acting element that localizes mRNA to synapses. *Proc. Natl. Acad. Sci. U. S. A.* **109**,
675 4639–4644 (2012).

676 37. R. B.-T. Perry, E. Doron-Mandel, E. Iavnilovitch, I. Rishal, S. Y. Dagan, M. Tsoory,
677 G. Coppola, M. K. McDonald, C. Gomes, D. H. Geschwind, J. L. Twiss, A. Yaron,
678 M. Fainzilber, Subcellular knockout of importin β1 perturbs axonal retrograde
679 signaling. *Neuron* **75**, 294–305 (2012).

680 38. D. Yan, Z. Wu, A. D. Chisholm, Y. Jin, The DLK-1 kinase promotes mRNA stability
681 and local translation in C. elegans synapses and axon regeneration. *Cell* **138**, 1005–
682 1018 (2009).

683 39. P. Sharifnia, K. W. Kim, Z. Wu, Y. Jin, Distinct cis elements in the 3' UTR of the C.
684 elegans cebp-1 mRNA mediate its regulation in neuronal development. *Dev. Biol.*
685 **429**, 240–248 (2017).

686 40. Z. Tan, Y. Fu, G. Sharma, D. H. Mathews, TurboFold II: RNA structural alignment
687 and secondary structure prediction informed by multiple homologs. *Nucleic Acids*
688 *Res.* **45**, 11570–11581 (2017).

689 41. A. P. Christensen, D. P. Corey, TRP channels in mechanosensation: direct or indirect
690 activation? *Nat. Rev. Neurosci.* **8**, 510–521 (2007).

691 42. J. L. Garrison, E. Z. Macosko, S. Bernstein, N. Pokala, D. R. Albrecht, C. I.
692 Bargmann, Oxytocin/Vasopressin-Related Peptides Have an Ancient Role in
693 Reproductive Behavior. *Science* **338**, 540–543 (2012).

694 43. N. G. Seidah, A. Prat, The biology and therapeutic targeting of the proprotein
695 convertases. *Nat. Rev. Drug Discov.* **11**, 367–383 (2012).

696 44. T. A. Lagace, D. E. Curtis, R. Garuti, M. C. McNutt, S. W. Park, H. B. Prather, N. N.
697 Anderson, Y. K. Ho, R. E. Hammer, J. D. Horton, Secreted PCSK9 decreases the
698 number of LDL receptors in hepatocytes and in livers of parabiotic mice. *J. Clin.*
699 *Invest.* **116**, 2995–3005 (2006).

700 45. D.-W. Zhang, T. A. Lagace, R. Garuti, Z. Zhao, M. McDonald, J. D. Horton, J. C.
701 Cohen, H. H. Hobbs, Binding of proprotein convertase subtilisin/kexin type 9 to
702 epidermal growth factor-like repeat A of low density lipoprotein receptor decreases
703 receptor recycling and increases degradation. *J. Biol. Chem.* **282**, 18602–18612
704 (2007).

705 46. S. Poirier, G. Mayer, The biology of PCSK9 from the endoplasmic reticulum to
706 lysosomes: new and emerging therapeutics to control low-density lipoprotein
707 cholesterol. *Drug Des. Devel. Ther.* **7**, 1135–1148 (2013).

708 47. S. Poirier, A. Prat, E. Marcinkiewicz, J. Paquin, B. P. Chitramuthu, D. Baranowski,
709 B. Cadieux, H. P. J. Bennett, N. G. Seidah, Implication of the proprotein convertase

710 NARC-1/PCSK9 in the development of the nervous system. *J. Neurochem.* **98**, 838–
711 850 (2006).

712 48. S. Antonacci, D. Forand, M. Wolf, C. Tyus, J. Barney, L. Kellogg, M. A. Simon, G.
713 Kerr, K. L. Wells, S. Younes, N. T. Mortimer, E. C. Olesnicky, D. J. Killian,
714 Conserved RNA-binding proteins required for dendrite morphogenesis in
715 Caenorhabditis elegans sensory neurons. *G3 Bethesda Md* **5**, 639–653 (2015).

716 49. Y. Hou, W. Liang, J. Zhang, Q. Li, H. Ou, Z. Wang, S. Li, X. Huang, C. Zhao,
717 Schizophrenia-associated rs4702 G allele-specific downregulation of FURIN
718 expression by miR-338-3p reduces BDNF production. *Schizophr. Res.* **199**, 176–
719 180 (2018).

720 50. S. Brenner, The genetics of Caenorhabditis elegans. *Genetics* **77**, 71–94 (1974).

721 51. C. Mello, A. Fire, "Chapter 19 DNA Transformation" in *Methods in Cell Biology*
722 (Elsevier, 1995;
723 https://linkinghub.elsevier.com/retrieve/pii/S0091679X08613990)vol. 48, pp. 451–
724 482.

725 52. J. A. Arribere, R. T. Bell, B. X. H. Fu, K. L. Artiles, P. S. Hartman, A. Z. Fire,
726 Efficient marker-free recovery of custom genetic modifications with CRISPR/Cas9
727 in Caenorhabditis elegans. *Genetics* **198**, 837–846 (2014).

728 53. Y. Zou, H. Chiu, A. Zinovyeva, V. Ambros, C.-F. Chuang, C. Chang, Developmental
729 decline in neuronal regeneration by the progressive change of two intrinsic timers.
730 *Science* **340**, 372–376 (2013).

731 54. H. Chiu, Y. Zou, N. Suzuki, Y.-W. Hsieh, C.-F. Chuang, Y.-C. Wu, C. Chang,
732 Engulfing cells promote neuronal regeneration and remove neuronal debris through
733 distinct biochemical functions of CED-1. *Nat. Commun.* **9**, 4842 (2018).

734 55. K. S. Liu, P. W. Sternberg, Sensory regulation of male mating behavior in
735 caenorhabditis elegans. *Neuron* **14**, 79–89 (1995).

736

737 **Figure 1. *kpc-1(xr58)* mutations preferentially affect PVD dendrite self-avoidance.** (a,
738 c) Images of PVD dendrites in wild type (a) and *xr58* mutants (c). Scale bar, 20 μm. (b)
739 Schematic of dendrites (green) and axon (grey) extended from a PVD neuron. PVD
740 projected primary (1°) dendritic processes anteriorly and posteriorly from the soma. Higher
741 order dendritic branching (secondary 2°, tertiary 3°, quaternary 4°) alternated between
742 anterior-posterior and dorsal-ventral directions to generate a regularly spaced array of
743 parallel branches. *xr58* mutants, while showing effective secondary dendrite branching,
744 displayed extensive defects in self-avoidance of sibling dendrites. Arrows point to contacts
745 between neighboring secondary dendrites. Arrowheads point to contacts between
746 neighboring tertiary dendrites. (d) Tertiary branch avoidance index (TBAI) in wild type
747 versus *kpc-1(xr58)* mutants. *kpc-1(xr58)* mutants displayed significantly lower TBAI than
748 wild-type animals. ***$p < 0.001$ by a Student's *t*-test. (e) Schematic of the KPC-1 protein
749 motifs showing locations of *xr47*, *xr58*, and *xr60* mutations. (f) Scatter plots showing the
750 positions of 4° dendrite termini in wild-type young adults and *kpc-1(xr58)* young adults.
751 In each scatter plot, the top line (dorsal nerve cord), the bottom line (ventral nerve cord),
752 and the wild-type PVD axon and primary dendrite (green) are shown.

753 **Figure 2. *kpc-1* is required for both secondary dendrite branching and tertiary**
754 **dendrite self-avoidance but the requirements of two functions are different.** (a) *kpc-1*
755 functions in PVD neurons to promote secondary dendrite branching largely independent of
756 the *kpc-1* 3'UTR. Percentage PVD neurons with secondary dendrite branching in *kpc-*
757 *1(gk8)* mutants carrying various transgenes. ***$p < 0.001$ by a two-proportion *Z*-test. (b)
758 The *kpc-1*'s function in PVD for tertiary dendrite self-avoidance is dependent on the *kpc-*
759 *1* 3'UTR. Percentage PVD neurons with defective tertiary dendrite self-avoidance in *kpc-*
760 *1(gk8)* and *kpc-1(xr58)* mutants carrying various transgenes. ND, not determined. ***$p <$
761 0.001 by a two-proportion *Z*-test. (c) Identification of the *kpc-1* promoter reporter
762 expression in PVD neurons. (d) Images of PVD neurons in *kpc-1(gk8)* mutants with or
763 without the *Ppvd::kpc-1::unc-54 3'UTR* transgene. The *Ppvd::kpc-1::unc-54 3'UTR*
764 transgene rescued the secondary dendrite branching but not the tertiary dendrite self-
765 avoidance defect in *kpc-1(gk8)* mutants. Arrowheads point to contacts between
766 neighboring tertiary dendrites. Asterisks indicate contacts between neighboring secondary
767 dendrites. (e, f) Images of PVD neurons in *kpc-1(gk8)* mutants without or with the
768 *Ppvd::kpc-1::kpc-1 3'UTR* transgene. The *Ppvd::kpc-1::kpc-1 3'UTR* transgene rescued
769 both the secondary dendrite branching and the tertiary dendrite self-avoidance defect in
770 *kpc-1(gk8)* mutants. (g, h) Images of PVD neurons in *kpc-1(xr58)* mutants without or with
771 the *Ppvd::kpc-1::kpc-1 3'UTR* transgene. The *Ppvd::kpc-1::kpc-1 3'UTR* transgene
772 rescued the tertiary dendrite self-avoidance defect in *kpc-1(xr58)* mutants. Arrowheads
773 point to contacts between neighboring tertiary dendrites. Scale bar, 20 μm.

774 **Figure 3. The *kpc-1* 3'UTR targets the *kpc-1* mRNA to higher-order dendrites.** (**a**) The
775 MS2 tagging system is composed of the *kpc-1* mRNA containing its own 3'UTR or a
776 control *unc-54* 3'UTR fused to 6xMS2 binding sites co-expressed with a green fluorescent
777 MS2 capsid protein. The nuclear localization signal (NLS) is used to initially target green
778 fluorescent MS2 proteins to the nucleus. (**b**) Image of the PVD neuron showing enriched
779 nuclear signals for the nuclear localized green fluorescent MS2 capsid protein. Asterisk
780 indicates soma. Scale bar, 20 μm. (**c**) Image of the PVD neuron showing axonal and
781 dendritic signals for *kpc-1* transcripts containing the *kpc-1* 3'UTR and MS2 binding sites.
782 The white arrow points to dendritic signals in the primary dendrite and the grey arrow
783 marks axonal signals. Grey arrowheads indicate the potential branching points at 3°
784 dendrites and contact points between neighboring 3° dendrites. The dashed box area in 3**c**
785 was blown up and shown in 3**d**. Anterior is to the left, dorsal is up. Scale bar, 20 μm. (**e**)
786 Image of the PVD neuron showing axonal and dendritic signals for *kpc-1* transcripts
787 containing the *kpc-1* 3'UTR and MS2 binding sites. Low level of the mCherry protein was
788 used to label PVD. Arrowheads point to potential tertiary dendrite contact points and open
789 arrowheads denote dendrite branching points. Arrows show red dendrite markers that are
790 not overlapped with any green MS2::GFP signals, indicating that red signals did not bleed
791 through to give rise to green signals. Scale bar, 20 μm. (**f**) Image of the PVD neuron
792 showing enriched soma signals for *kpc-1* transcripts containing the control *unc-54* 3'UTR
793 and MS2 binding sites. Asterisk indicates soma. Scale bar, 20 μm. (**g**) Average number of
794 punctate MS2 fluorescence signals on 3° dendrites in transgenic animals expressing *kpc-1*
795 transcripts, containing either its own 3'UTR or the control *unc-54* 3'UTR. ***$p < 0.001$
796 by a Student's *t*-test. (**h**) Percentage PVD neurons with punctate MS2 fluorescence signals

797 on 3° dendrites in transgenic animals expressing *kpc-1* transcripts, containing either its own

798 3'UTR or the control *unc-54* 3'UTR. ***$p < 0.001$ by a two-proportion *Z*-test.

799

800 **Figure 4. The *kpc-1* 3'UTR promotes local protein synthesis in the distal segment of**
801 **PVD dendrites.** (**a**) Representative images of Kaeda-labelled PVD dendrites pre- and post-
802 photoconversion. The dashed white box indicates a wide photoconverted region. The solid
803 yellow box denotes a targeted area of analysis, which is distal to the soma within the wide
804 photoconverted region. Scale bar, 20 μm. (**b**) Pre-photoconversion of resident Kaede
805 proteins and post-photoconversion of newly synthesized Kaede proteins. Kaeda expression
806 in PVD dendrites is controlled by either a control *unc-54* 3'UTR or a *kpc-1* 3'UTR. Scale
807 bar, 20 μm. (**c**) The *kaeda::kpc-1 3'UTR* transcript is expressed at a higher rate compared
808 to the control *kaeda::unc-54 3'UTR* transcript. Quantification of green signal recovery in
809 a targeted distal area after photoconversion of a wider region of PVD dendrites. Statistical
810 analysis using 2-way ANOVA. Average data of Kaeda expression intensity are presented
811 as means ± SEM. (**d**) Expression of a split GFP reporter allows visualization of ribosomes
812 in PVD neurons. The smaller part of split GFP (GFP11) is tagged to the endogenous *rps-*
813 *18* (GFP11::rps-18). The larger part of split GFP (GFP1-10) is overexpressed from a PVD
814 promoter *ser-2* using a high-copy transgene. GFP1-10 binds to the GFP11::RPS-18 in
815 neurons and illuminates RPS-18. The *Pser-2::mCherry* marker labels PVD dendrites.
816 Ribosomes are mostly restricted in the PVD soma, which is marked by an asterisk.
817 Arrowheads indicate RPS-18 signals. Scale bar, 20 μm.

818 **Figure 5. A putative stem-loop secondary structure in the *kpc-1* 3'UTR is required**
819 **for tertiary dendrite self-avoidance.** (**a**) Illustration of putative stem-loop secondary
820 structural motifs and specific mutations in the *kpc-1* 3'UTR. (**b-d**) Representative images
821 of the *kpc-1(gk8)* mutant, the *kpc-1(gk8)* mutant expressing the *Ppvd::kpc-1::kpc-1* 3'UTR
822 transgene (SLS2 mutated base pairing disrupted), and the *kpc-1(gk8)* mutant expressing
823 the *Ppvd::kpc-1::kpc-1* 3'UTR transgene (SLS2 mutated base pairing preserved).
824 Arrowheads point to contacts between neighboring tertiary dendrites. Scale bars, 20 μm.
825 (**e**) Percentage PVD neurons with defective secondary dendrite branching in wild-type,
826 *kpc-1(gk8)* mutants, and *kpc-1(gk8)* mutants carrying various transgenes. **$p < 0.01$ and
827 ***$p < 0.001$ by a two-proportion *Z*-test. (**f**) Quantification of contact points between
828 sibling tertiary dendrites in wild-type and *kpc-1(gk8)* mutants carrying various transgenes.
829 ND, not determined. ***$p<0.001$ by one-way ANOVA with Dunnett's test.

830 **Figure 6. *kpc-1* alleles differentially affect DMA-1 levels on 3° dendrites and 3°**
831 **dendrite self-avoidance.** (**a**) Representative images showing DMA-1::GFP expression on
832 PVD dendrites in wild type, *kpc-1(xr58)*, and *kpc-1(xr47)* mutants. Asterisk indicates
833 soma. Arrowheads indicate tertiary branches. Scale bars, 20 μm. (**b**) Average fluorescence
834 intensity of the DMA-1::GFP on PVD tertiary dendrites in wild type [*dma-1(wy1246)*],
835 *kpc-1(xr58)* mutants [*kpc-1(xr58); dma-1(wy1246)*], and *kpc-1(xr47)* mutants [*kpc-*
836 *1(xr47); dma-1(wy1246)*]. The *dma-1(wy1246) [dma-1::GFP]* allele was created by
837 inserting a GFP reporter gene immediately after the transmembrane domain of the
838 endogenous *dma*-1 gene. This reporter strain does not cause any defects in PVD
839 dendrites(*3*). **$p < 0.01$ and ***$p < 0.001$ by one-way ANOVA with Tukey's test. (**c**)
840 Quantification of overlapped tertiary dendrites in wild type versus *kpc-1* mutants. ***$p <$
841 0.001 by one-way ANOVA with Tukey's test. (**d**) Image of the trans-heterozygous *kpc-*
842 *1(xr58)/kpc-1(gk8)* mutant displaying self-avoidance defects similar to those displayed by
843 homozygous *kpc-1(xr58)* mutants. Scale bars, 20 μm.

844 **Figure 7. *dma-1* over-expression phenocopied the *kpc-1(xr58)* mutant allele.** (a, b)
845 Images of PVD dendrites in *kpc-1(xr58)* mutants and *dma-1* over-expression animals.
846 Arrowheads point to contacts between neighboring tertiary dendrites. Scale bars, 20 μm.
847 (c-e) Images of PVD dendrites in *kpc-1* over-expression animals, *dma-1* over-expression
848 animals, and animals over-expressing both *kpc-1* and *dma-1*. Scale bars, 20 μm. (f) *kpc-1*
849 over-expression suppressed secondary dendrite branching phenotypes in *dma-1* over-
850 expression animals. (g, h) Images of PVD neurons showing dendritic signals for *kpc-1*
851 transcripts and DMA-1 proteins. *kpc-1* transcripts containing *kpc-1* 3'UTR and MS2
852 binding sites were visualized by green fluorescent MS2 capsid proteins. DMA-1 proteins
853 were visualized by tagged mCherry fluorescent proteins. White arrowheads point to
854 dendritic signals for *kpc-1* transcripts and grey arrowheads indicate dendritic signals for
855 DMA-1 proteins. Scale bars, 15 μm. (i) Bar chart of average PVD dendrite length in wild
856 type and *kpc-1(xr58)* mutants. Dendritomy was carried out at the early L4 stage when
857 tertiary dendrites underwent self-avoidance. Newly grown PVD dendrite length was
858 measured 24 hours after dendritomy. P=0.83 by a Student's *t*-test. Error bars indicate SEM.
859 (j) Bar chart of average distances between neighboring tertiary dendrites in wild type and
860 *kpc-1* over-expression animals at the young adult stage. For each animal, average distances
861 of the gaps between neighboring tertiary dendrites were measured per 150 μm anterior to
862 the cell body. *kpc-1* over-expression animals differ from wild-type at **p<0.01 by a
863 Student's *t*-test. Error bars indicate SEM. (k) Model of the *kpc-1-dma-1* regulatory circuit
864 in dendrite branching and self-avoidance. *kpc-1* is expressed at branching points and
865 contact points between the neighboring 3° dendrites, which down-regulates DMA-1

866 receptors locally, leading to dendrite branching and retraction of sibling dendrites. SAX-7

867 cues are distributed highly in the 1° and the 3° dendrite growth pathways.

868 **Figure 8. *kpc-1* mutant males exhibit mating defects.** (**a**) Images of PVD dendrites in
869 wild-type and *kpc-1(xr58)* mutant males. Arrowheads point to contacts between
870 neighboring tertiary dendrites. Scale bars, 20 μm. (**b**) Tertiary branch avoidance index of
871 the wild-type and *kpc-1(xr58)* mutant males. ***$p < 0.001$ by a Student's *t*-test. (**c**)
872 Receptive field index of the wild-type and *kpc-1(xr58)* mutant males. Receptive field
873 index was defined by the ratio of the skin area innervated by the dendrite arbors
874 normalized to the skin area of the animal body, measured from the PVD soma to the end
875 of the mouth (anterior most point in the animal). ***$p < 0.001$ by a Student's *t*-test. (**d**)
876 Reproductive efficiencies of wild-type and *kpc-1(xr58)* mutant males. Three repeats were
877 performed for each strain. **$p < 0.01$ by a Student's *t*-test. (**e**) The number of
878 hermaphrodites contacted by males before mating initiation. $p = 0.86$ by a Student's *t*-
879 test. (**f**) The number of turns the males made around hermaphrodites' head and tail before
880 locating the vulva. **$p < 0.01$ by a Student's *t*-test. Error bars, SEM.

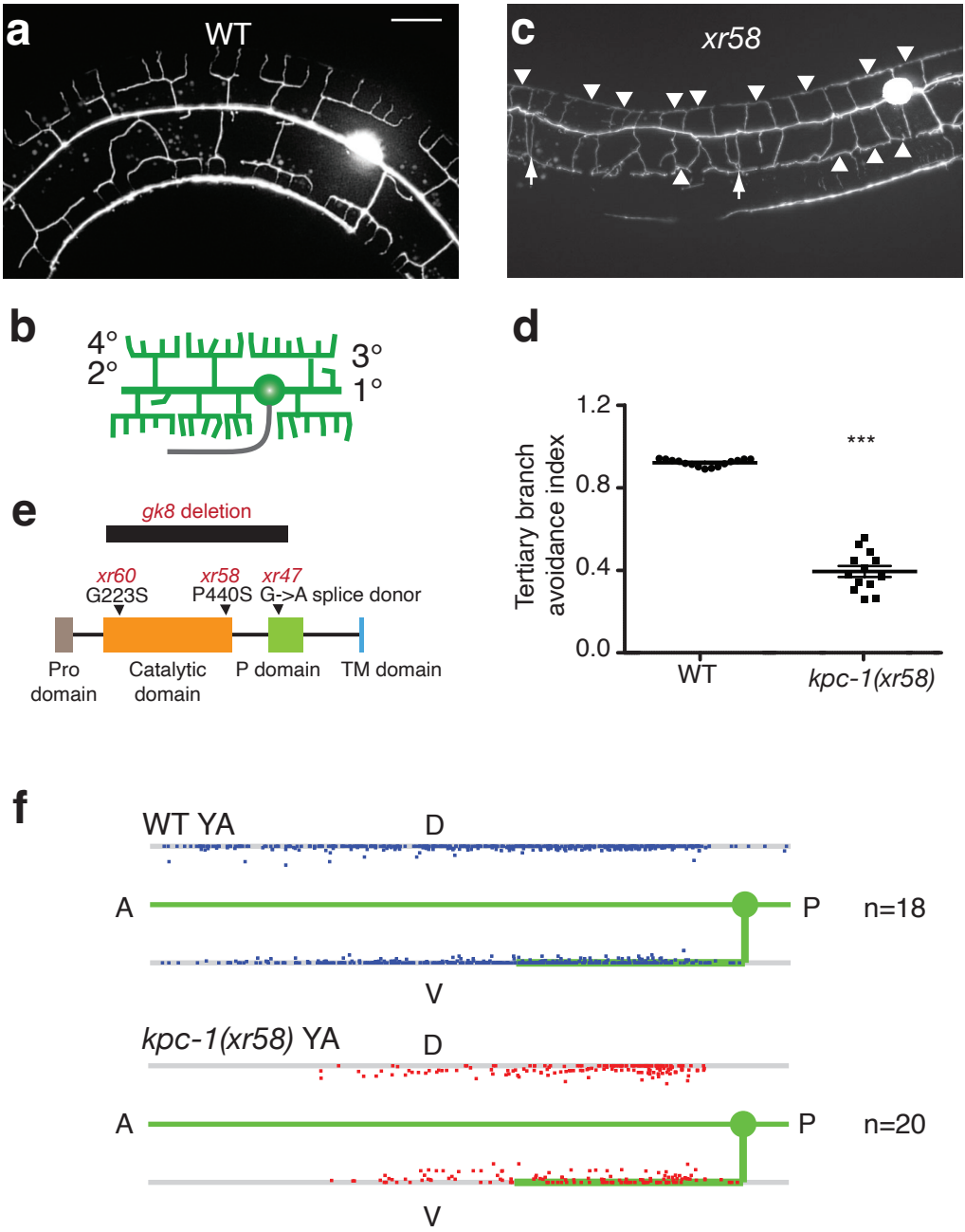
a
WT
c
xr58
b
4°
2°
3°
1°
d
Tertiary branch avoidance index
1.2
0.8
0.4
0.0
***
WT
kpc-1(xr58)
e
gk8 deletion
xr60
G223S
xr58
P440S
xr47
G->A splice donor
Pro domain
Catalytic domain
P domain
TM domain
f
WT YA
D
A
P
n=18
V
kpc-1(xr58) YA
D
A
P
n=20
V

Figure 1

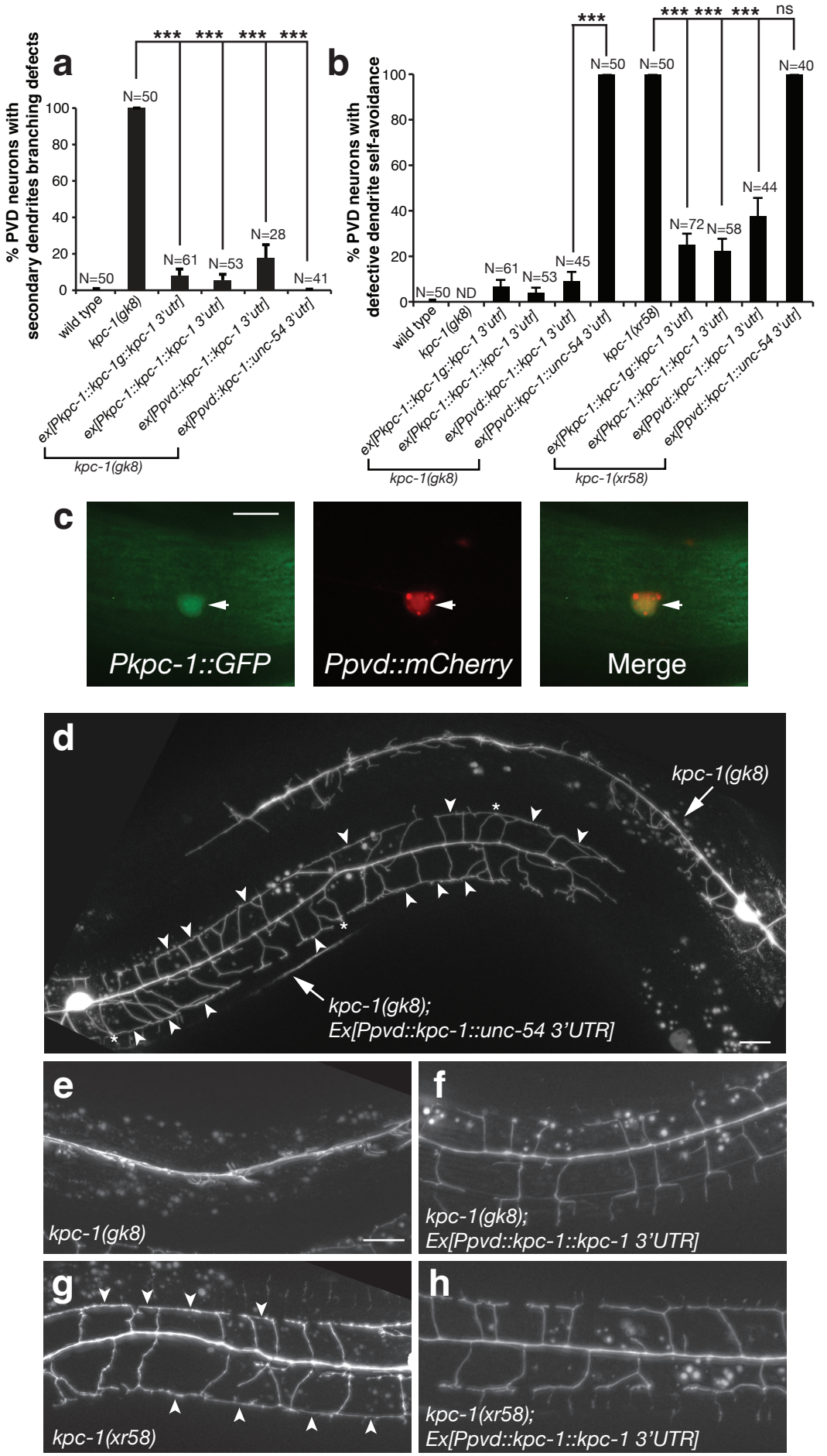
a
% PVD neurons with secondary dendrites branching defects
***
N=50
N=61
N=53
N=28
N=41
wild type
kpc-1(gk8)
ex[Pkpc-1::kpc-1g::kpc-1 3'utr]
ex[Pkpc-1::kpc-1::kpc-1 3'utr]
ex[Ppvd::kpc-1::kpc-1 3'utr]
ex[Ppvd::kpc-1::unc-54 3'utr]
kpc-1(gk8)
b
% PVD neurons with defective dendrite self-avoidance
***
ns
N=50
ND
N=61
N=53
N=45
N=50
N=50
N=72
N=58
N=44
N=40
kpc-1(xr58)
c
Pkpc-1::GFP
Ppvd::mCherry
Merge
d
kpc-1(gk8)
kpc-1(gk8);
Ex[Ppvd::kpc-1::unc-54 3'UTR]
e
kpc-1(gk8)
f
kpc-1(gk8);
Ex[Ppvd::kpc-1::kpc-1 3'UTR]
g
kpc-1(xr58)
h
kpc-1(xr58);
Ex[Ppvd::kpc-1::kpc-1 3'UTR]

Figure 2

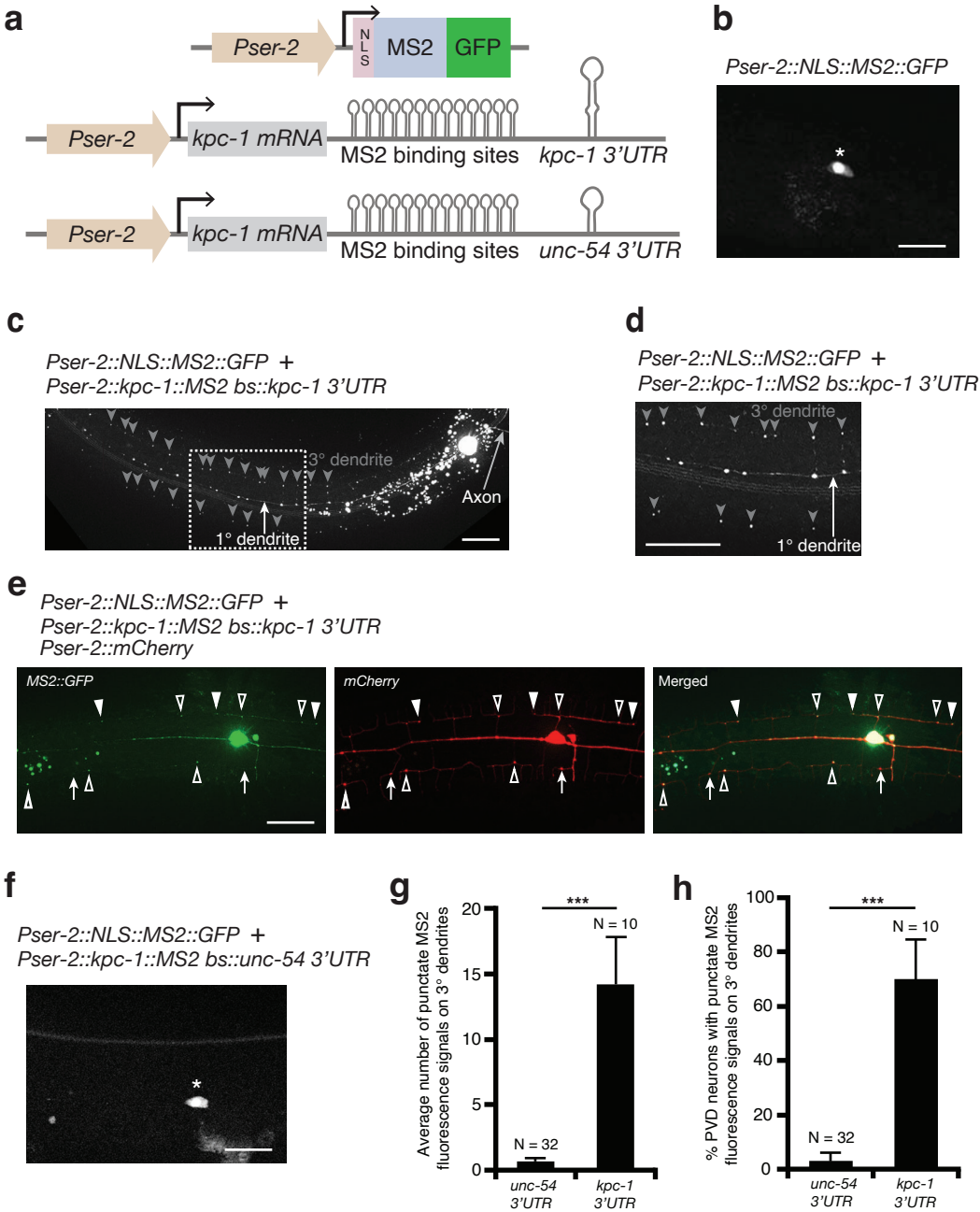
a
Pser-2
NLS
MS2
GFP
Pser-2
kpc-1 mRNA
MS2 binding sites
kpc-1 3'UTR
Pser-2
kpc-1 mRNA
MS2 binding sites
unc-54 3'UTR
b
Pser-2::NLS::MS2::GFP
c
Pser-2::NLS::MS2::GFP +
Pser-2::kpc-1::MS2 bs::kpc-1 3'UTR
3° dendrite
Axon
1° dendrite
d
Pser-2::NLS::MS2::GFP +
Pser-2::kpc-1::MS2 bs::kpc-1 3'UTR
3° dendrite
1° dendrite
e
Pser-2::NLS::MS2::GFP +
Pser-2::kpc-1::MS2 bs::kpc-1 3'UTR
Pser-2::mCherry
MS2::GFP
mCherry
Merged
f
Pser-2::NLS::MS2::GFP +
Pser-2::kpc-1::MS2 bs::unc-54 3'UTR
g
Average number of punctate MS2 fluorescence signals on 3° dendrites
***
N = 10
N = 32
unc-54 3'UTR
kpc-1 3'UTR
h
% PVD neurons with punctate MS2 fluorescence signals on 3° dendrites
***
N = 10
N = 32
unc-54 3'UTR
kpc-1 3'UTR

Figure 3

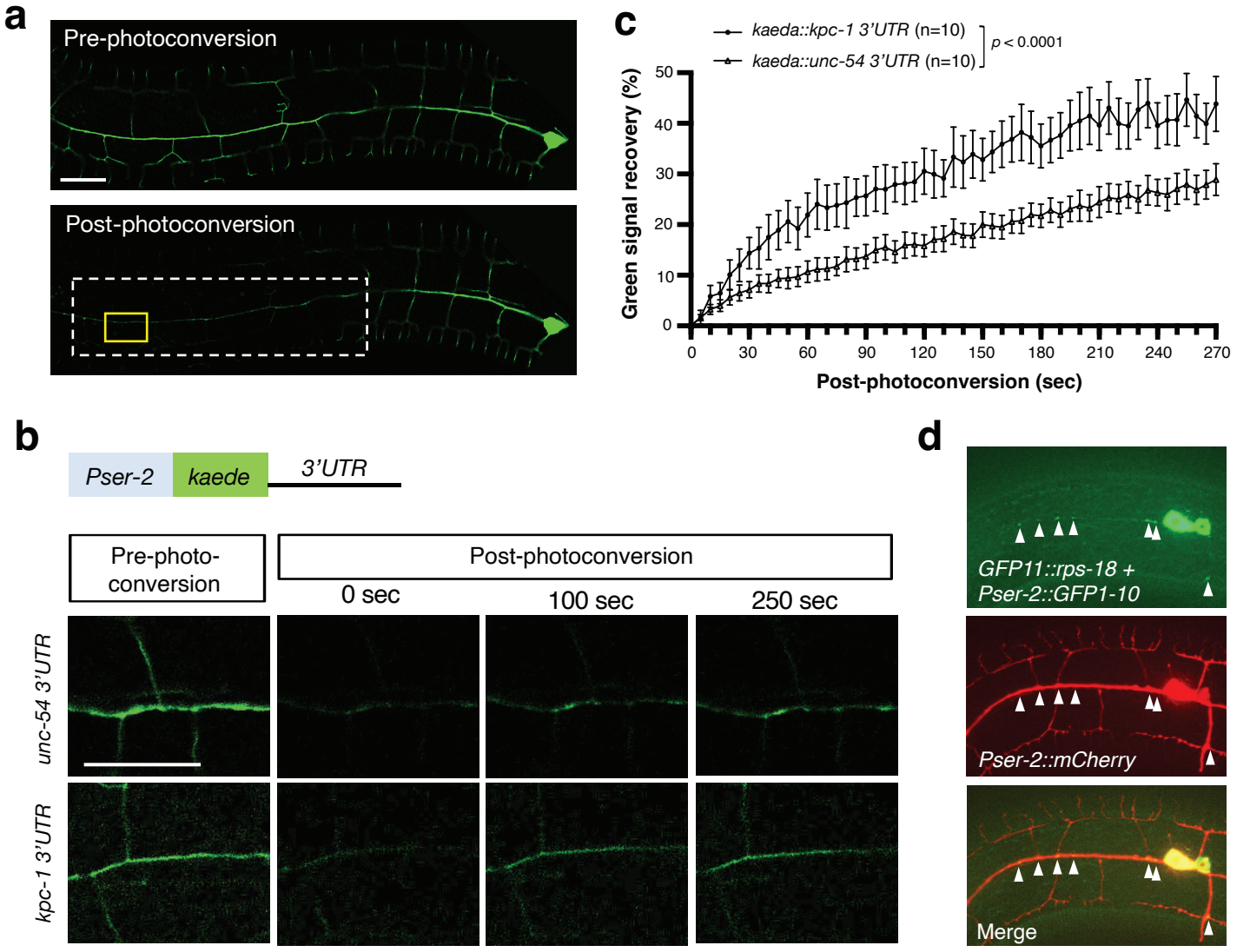
a
Pre-photoconversion
Post-photoconversion
c
kaeda::kpc-1 3'UTR (n=10)
kaeda::unc-54 3'UTR (n=10)
p < 0.0001
Green signal recovery (%)
Post-photoconversion (sec)
b
Pser-2
kaede
3'UTR
Pre-photo-conversion
Post-photoconversion
0 sec
100 sec
250 sec
unc-54 3'UTR
kpc-1 3'UTR
d
GFP11::rps-18 +
Pser-2::GFP1-10
Pser-2::mCherry
Merge

Figure 4

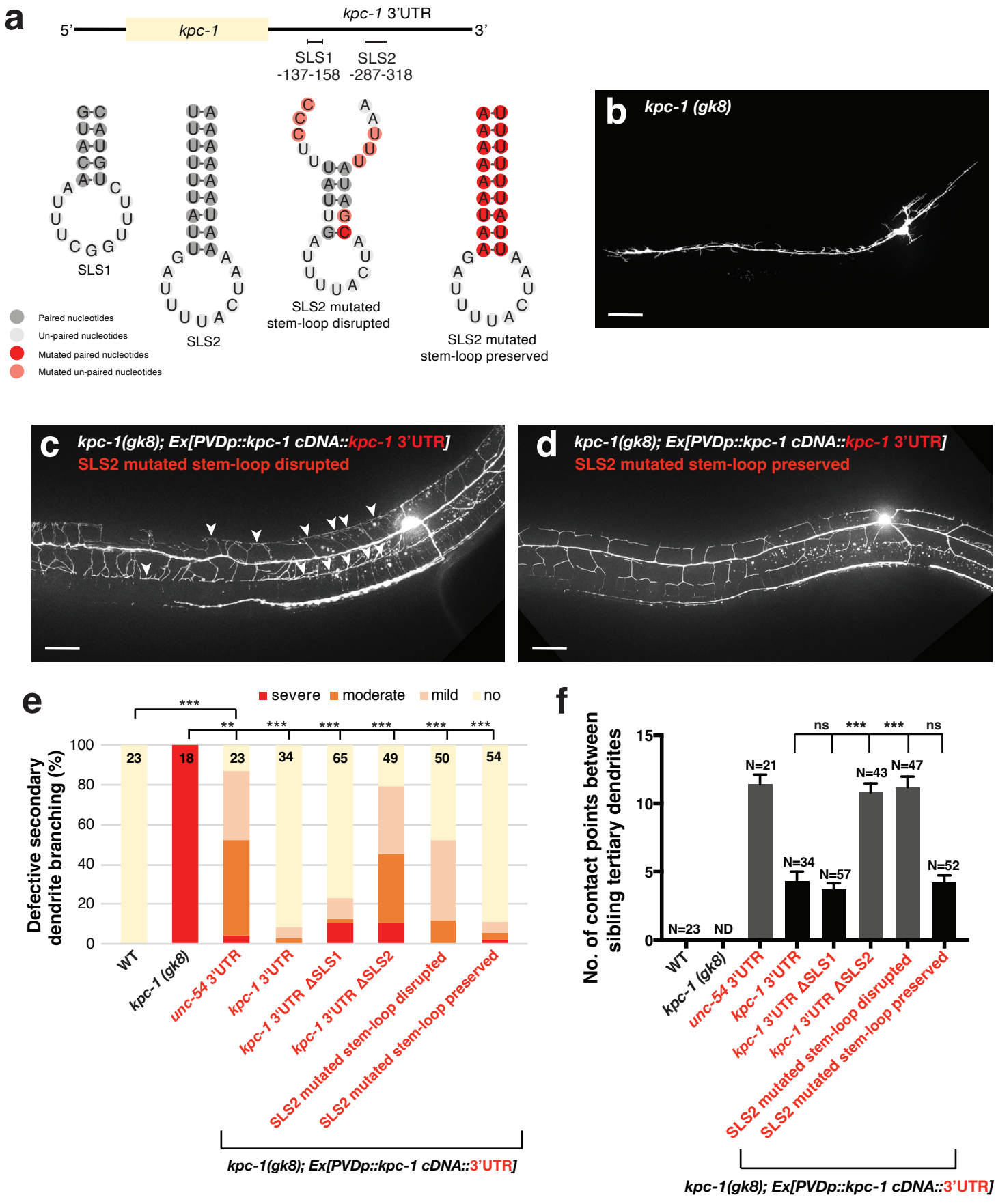
a
5'
kpc-1
kpc-1 3'UTR
3'
SLS1
-137-158
SLS2
-287-318
SLS1
SLS2
SLS2 mutated
stem-loop disrupted
SLS2 mutated
stem-loop preserved
Paired nucleotides
Un-paired nucleotides
Mutated paired nucleotides
Mutated un-paired nucleotides
b
kpc-1 (gk8)
c
kpc-1(gk8); Ex[PVDp::kpc-1 cDNA::kpc-1 3'UTR]
SLS2 mutated stem-loop disrupted
d
kpc-1(gk8); Ex[PVDp::kpc-1 cDNA::kpc-1 3'UTR]
SLS2 mutated stem-loop preserved
e
severe
moderate
mild
no
Defective secondary dendrite branching (%)
100
80
60
40
20
0
23
18
23
34
65
49
50
54
***
**
***
***
***
***
***
WT
kpc-1 (gk8)
unc-54 3'UTR
kpc-1 3'UTR
kpc-1 3'UTR ΔSLS1
kpc-1 3'UTR ΔSLS2
SLS2 mutated stem-loop disrupted
SLS2 mutated stem-loop preserved
kpc-1(gk8); Ex[PVDp::kpc-1 cDNA::3'UTR]
f
No. of contact points between sibling tertiary dendrites
15
10
5
0
N=23
ND
N=21
N=34
N=57
N=43
N=47
N=52
ns
***
***
ns
WT
kpc-1 (gk8)
unc-54 3'UTR
kpc-1 3'UTR
kpc-1 3'UTR ΔSLS1
kpc-1 3'UTR ΔSLS2
SLS2 mutated stem-loop disrupted
SLS2 mutated stem-loop preserved
kpc-1(gk8); Ex[PVDp::kpc-1 cDNA::3'UTR]

Figure 5

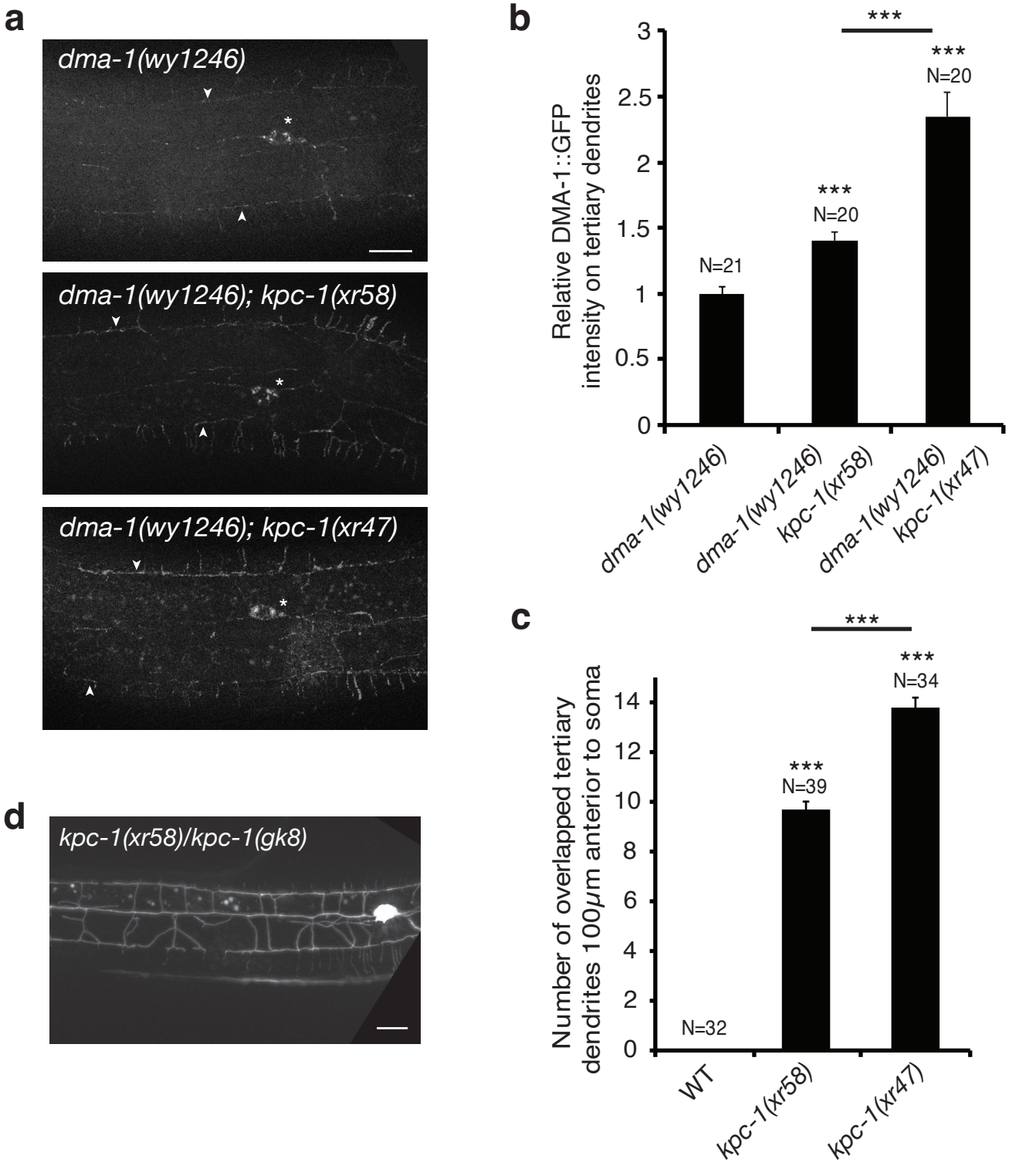
a
dma-1(wy1246)
dma-1(wy1246); kpc-1(xr58)
dma-1(wy1246); kpc-1(xr47)
b
Relative DMA-1::GFP intensity on tertiary dendrites
0
0.5
1
1.5
2
2.5
3
***
***
N=20
***
N=20
N=21
dma-1(wy1246)
dma-1(wy1246) kpc-1(xr58)
dma-1(wy1246) kpc-1(xr47)
c
Number of overlapped tertiary dendrites 100μm anterior to soma
0
2
4
6
8
10
12
14
***
***
N=34
***
N=39
N=32
WT
kpc-1(xr58)
kpc-1(xr47)
d
kpc-1(xr58)/kpc-1(gk8)

Figure 6

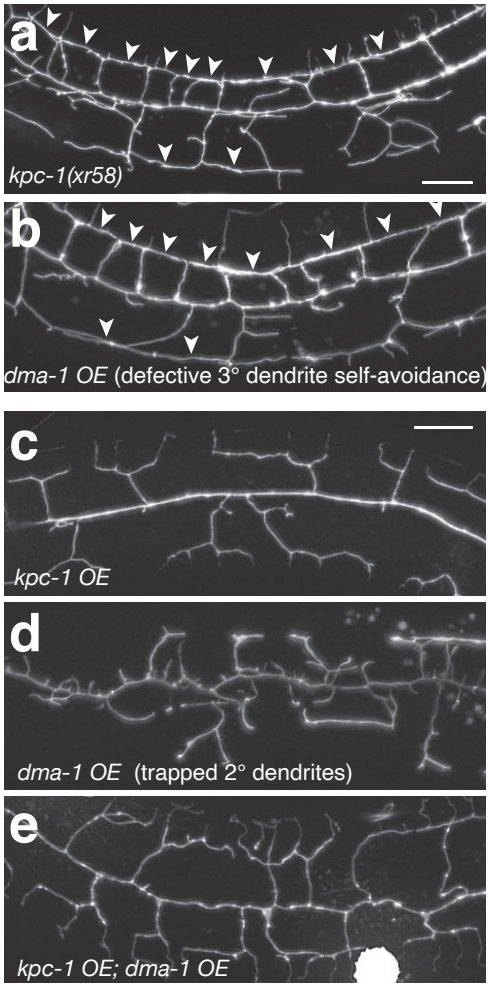
a
kpc-1(xr58)
b
dma-1 OE (defective 3° dendrite self-avoidance)
c
kpc-1 OE
d
dma-1 OE (trapped 2° dendrites)
e
kpc-1 OE; dma-1 OE

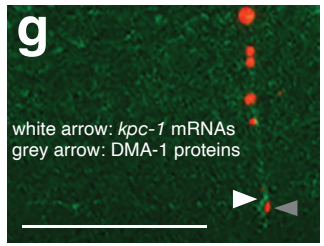
g
white arrow: kpc-1 mRNAs
grey arrow: DMA-1 proteins

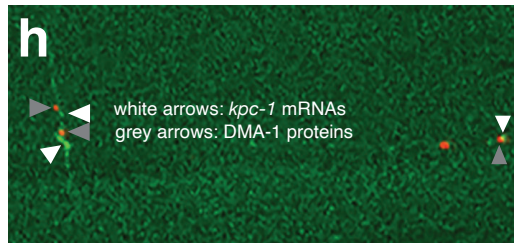
h
white arrows: kpc-1 mRNAs
grey arrows: DMA-1 proteins

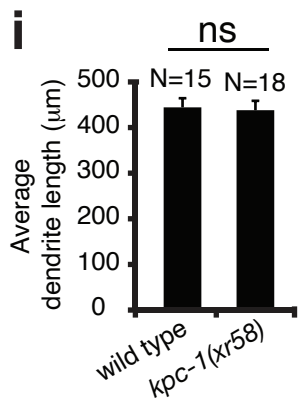
i
ns
N=15
N=18
Average dendrite length (µm)
500
400
300
200
100
0
wild type
kpc-1(xr58)

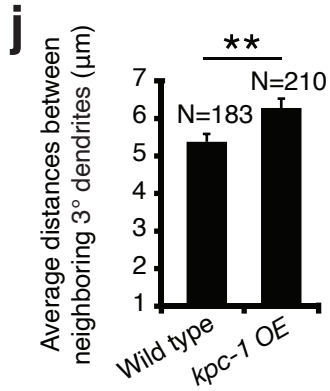
j
**
N=183
N=210
Average distances between neighboring 3° dendrites (µm)
7
6
5
4
3
2
1
Wild type
kpc-1 OE

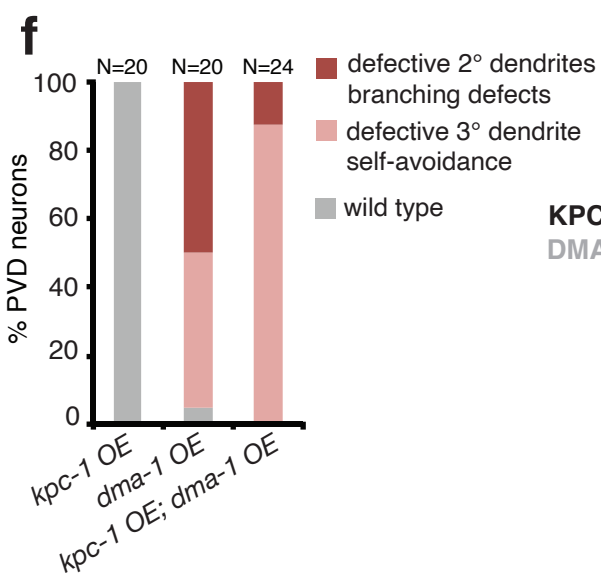
f
N=20
N=20
N=24
% PVD neurons
100
80
60
40
20
0
defective 2° dendrites branching defects
defective 3° dendrite self-avoidance
wild type
kpc-1 OE
dma-1 OE
kpc-1 OE; dma-1 OE

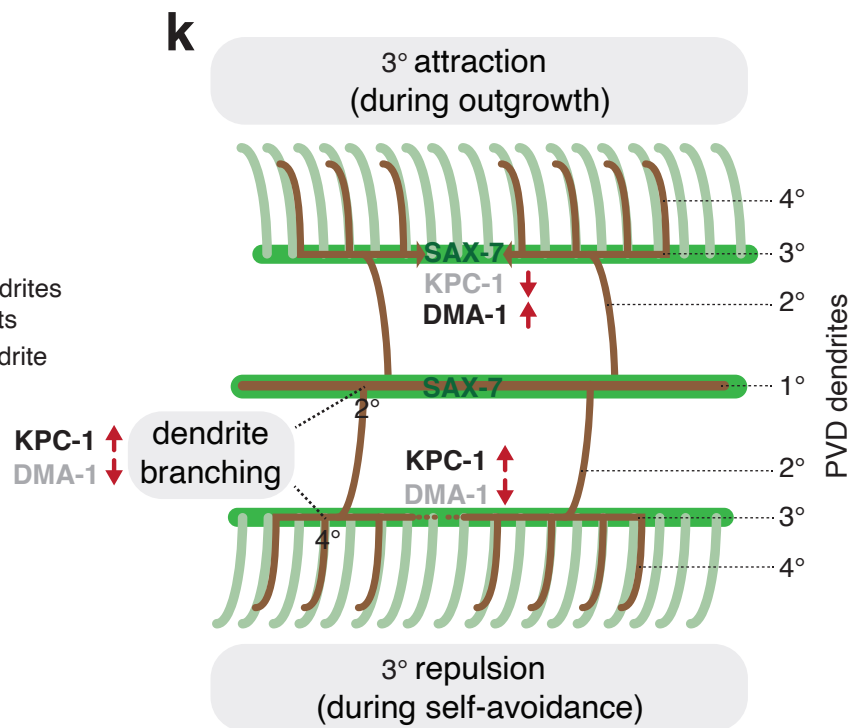
k
3° attraction
(during outgrowth)
4°
3°
SAX-7
KPC-1
DMA-1
2°
SAX-7
1°
2°
KPC-1
DMA-1
dendrite branching
KPC-1
DMA-1
2°
3°
4°
4°
PVD dendrites
3° repulsion
(during self-avoidance)

Figure 7

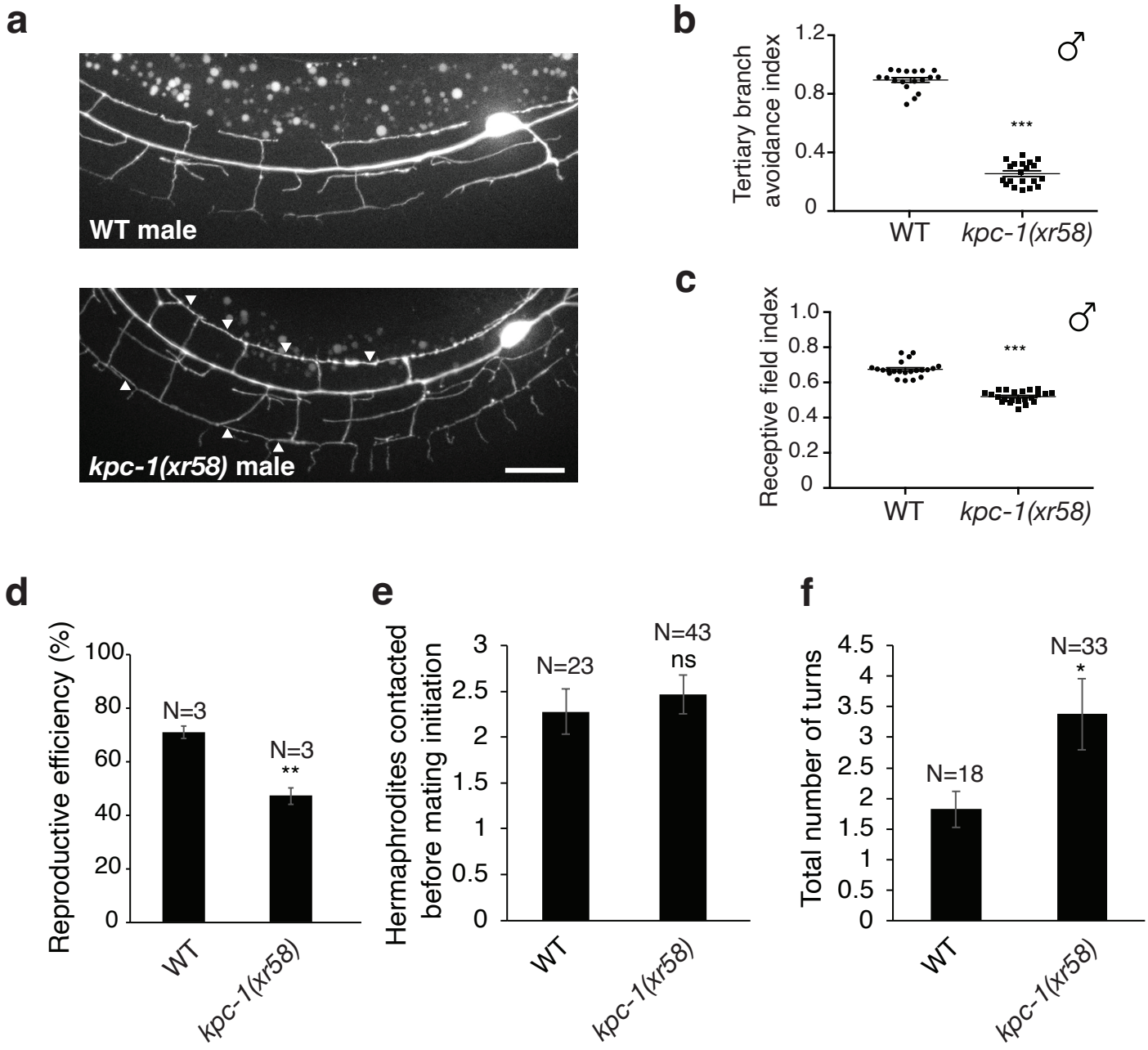
a
WT male
kpc-1(xr58) male
b
Tertiary branch avoidance index
1.2
0.8
0.4
0
***
WT
kpc-1(xr58)
c
Receptive field index
1.0
0.8
0.6
0.4
0.2
0
***
WT
kpc-1(xr58)
d
Reproductive efficiency (%)
100
80
60
40
20
0
N=3
N=3
**
WT
kpc-1(xr58)
e
Hermaphrodites contacted before mating initiation
3
2.5
2
1.5
1
0.5
0
N=23
N=43
ns
WT
kpc-1(xr58)
f
Total number of turns
4.5
4
3.5
3
2.5
2
1.5
1
0.5
0
N=18
N=33
*
WT
kpc-1(xr58)

Figure 8

Genotype	N	Menorah coverage zone per 200 μm of 1° dendrite	Trapped 2° dendrite zone per 200 μm of 1° dendrite
Wild type	32	183.99	0
kpc-1(xr58)	39	182.88	38.51
kpc-1(xr47)	32	143.46	73.18
kpc-1(xr60)	27	58.73	163.90
kpc-1(gk8)	32	3.14	196.86